

PCCP

Accepted Manuscript



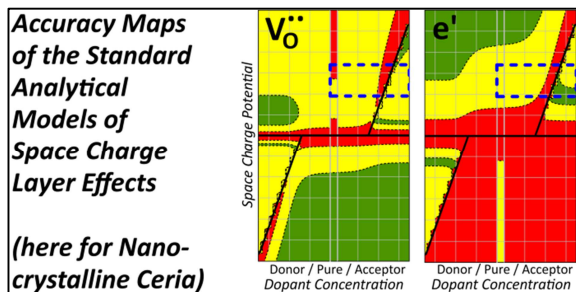
This is an *Accepted Manuscript*, which has been through the Royal Society of Chemistry peer review process and has been accepted for publication.

Accepted Manuscripts are published online shortly after acceptance, before technical editing, formatting and proof reading. Using this free service, authors can make their results available to the community, in citable form, before we publish the edited article. We will replace this *Accepted Manuscript* with the edited and formatted *Advance Article* as soon as it is available.

You can find more information about *Accepted Manuscripts* in the [Information for Authors](#).

Please note that technical editing may introduce minor changes to the text and/or graphics, which may alter content. The journal's standard [Terms & Conditions](#) and the [Ethical guidelines](#) still apply. In no event shall the Royal Society of Chemistry be held responsible for any errors or omissions in this *Accepted Manuscript* or any consequences arising from the use of any information it contains.

Graphical abstract Part I



Using numerical calculations the reliability of the standard analytical models of space charge effects is evaluated; improved solutions are proposed.

Numerical Calculations of Space Charge Layer Effects in Nanocrystalline Ceria. Part I: Comparison with the Analytical Models and Derivation of Improved Analytical Solutions

Marcus C. Göbel, Giuliano Gregori,¹ Joachim Maier

Max Planck Institute for Solid State Research, Heisenbergstr. 1, D-70569 Stuttgart, Germany

Abstract

Using numerical solutions of the Poisson-equation, one dimensional space charge layer (SCL) concentration profiles in CeO₂ are calculated. The SCL conductivity effects of nanocrystalline CeO₂ are analyzed as a function of doping content (donor doped, pure and acceptor doped ceria) and SCL potential including not only the standard Gouy-Chapman and Mott-Schottky cases, but also the more complex mixed situations. The results of the numerical approach are compared with the usual analytical approximations. While for the ideal Gouy-Chapman and Mott-Schottky cases for moderate and high potentials the agreement between analytical and numerical solutions is found to be satisfactory, mixed cases and low potential situations cannot be reliably treated by using the standard analytical approaches. Finally, inspired from the numerical solutions, improved analytical equations are proposed which are found to generally yield much more precise results and are accurate even for the mixed situations and low potentials.

¹ Corresponding author
E-mail address: g.gregori@fkf.mpg.de, s.weiglein@fkf.mpg.de
Fax: +49-711-689-1722

1 Introduction

Space charge layers (SCLs) in ionic conductors are of major importance for both basic research and applications.¹⁻³ For many materials SCLs were found to drastically change the electrical transport properties at both homo⁴ and hetero-junctions.⁵ The origin of the SCLs at the grain boundaries (GBs) is generally explained in terms of an electrically charged interface core, due to a deviation from the bulk cation-to-anion ratio or due to extrinsic effects such as excess or deficiency of dopants. The resulting core charge Σ_{Core} leads, in the surrounding material, to the enrichment of oppositely and the depletion of likewise charged charge carriers. As a consequence, the core charge Σ_{Core} is balanced by two SCL charges (Σ_{SCL}), i.e. the global electroneutrality condition is fulfilled, as schematically shown in **Fig. 1**:

$$\Sigma_{SCL} = -\frac{1}{2}\Sigma_{Core} \quad \{1\}$$

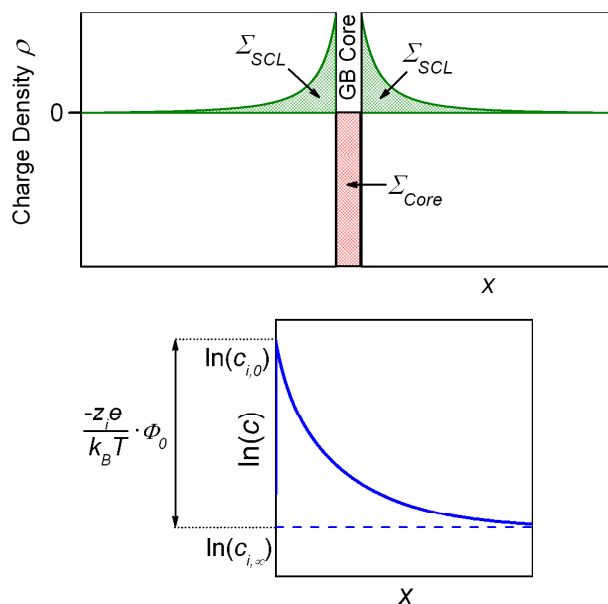


Fig. 1 Basic features of a SCL (here Gouy-Chapman case). Top panel: charge density ρ as a function of the distance x from the interface. Bottom panel: Charge carrier concentration $\ln(c)$ as a function of x .

For the exact definition of the different quantities please refer to **Table 1**. As long as the carrier concentration c_i is diluted,^{II} the equilibrium distribution in the space charge zone is given by

$$c_i = c_{i,\infty} \cdot e^{-\frac{z_i e}{k_B T} \Phi}, \quad \{2\}$$

where $c_{i,\infty}$ is the bulk concentration of the mobile charge carrier i , z_i its corresponding charge number, e the elementary charge, and $k_B T$ the Boltzmann term. Note that Φ is the deviation of the local electrical potential from the bulk value. The electric potential adjacent to the grain boundary core Φ_0 (namely for $x = 0$) is termed space charge potential. In the SCL the enrichment or depletion of charged defects (see eq. {2}) results in a local charge density ρ as graphically shown in **Fig. 1**:

$$\rho = e \cdot \sum_{i=1}^{N_M} (z_i c_i) + \rho_{IM} \quad \{3\}$$

$$\Sigma_{SCL} = \int_0^{+\infty} \rho \cdot dx = -\varepsilon_r \varepsilon_0 E_0. \quad \{4\}$$

Hereby ε_0 is the vacuum permittivity, ε_r the relative permittivity, E_0 the electric field at the interface, N the number of charge carriers, while the subscripts M and IM refer to the mobile and immobile charge carriers, respectively. Note that the concentrations of the immobile charge carriers $c_{IM,j}$, which are not able to follow the SCL potential are here considered as constant (and hence also their charge density ρ_{IM}).^{III}

$$\rho_{IM} = e \cdot \sum_{j=1}^{N_{IM}} (z_{IM,j} c_{IM,j}), \quad \{5\}$$

The local charge density is again connected with the electric potential via the Poisson-equation:

$$\frac{d^2 \Phi}{dx^2} = -\frac{\rho}{\varepsilon_r \varepsilon_0}. \quad \{6\}$$

^{II} In case of a very high potential (and in particular in combination with a high bulk concentration of the enriched charge carrier) eq. {2} can yield unrealistically high concentration values above 1. Such an unreasonably strong enrichment of charge carriers corresponds to an unrealistically high SCL charge and, hence, to an unrealistically high GB core charge (see eq. {1}). The limitations arising from the fact that the SCL and the core charges cannot surpass a certain physical limit (hence the situations in which eq. {2} is not valid), are discussed in detail in Part II of this contribution (Section 2.2).⁶

^{III} A study dealing with the more complex situation of a not flat profile of the immobile charge carriers is given in ref. 7.

In order to determine the potential profile function $\Phi(x)$ and, hence, also the concentration profile functions $c_i(x)$ (see eq. {2}) the Poisson-equation needs to be solved.

Before dealing with this aspect, it is well worth mentioning that a rearrangement and integration of eq. {6} (after eq. {2} and {3} have been inserted) yields the following analytical expression for Σ_{SCL} :

$$\Sigma_{SCL} = -\varepsilon_r \varepsilon_0 E_0 = -\text{sgn}(\Phi_0) \cdot \sqrt{2\varepsilon_r \varepsilon_0 k_B T \left(\sum_{i=1}^{N_M} \left(c_{i,\infty} \left(e^{\frac{-z_i e}{k_B T} \Phi_0} - 1 \right) \right) - \frac{\rho_{IM}}{k_B T} \Phi_0 \right)}. \quad \{7\}$$

The derivation of eq. {7} is given in the Supplementary Information. The key aspect is that eq. {7} is obtained without making use of any further simplifying assumptions. Hence, it allows for a reliable determination of the total SCL charge even for very complex situations and, quite remarkably, even if the SCL profile functions $\Phi(x)$ and $c_i(x)$ are unknown, given that for the derivation of eq. {7} the Poisson-equation does not need to be solved.

However, the analysis of the influence of SCL effects on the conduction properties of an ionic or mixed conductor requires the understanding of the precise profile functions (with very few exceptions). Usually, it is based on a series of analytical solutions – Gouy-Chapman (GC) and Mott-Schottky (MS) cases – which, nonetheless, present some limitations as they are valid under certain approximations.

In this study, we present instead a numerical approach to accurately solve the Poisson-equation of the SCL profiles. This approach deals with non-overlapping, one dimensional SCLs (a study of overlapping SCLs in ceria is given in ref. 8). The contribution is organized as follows:

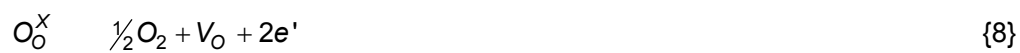
- (i) The results of the analytical approximations are presented for a broad range of dopant concentrations and space charge potentials with the purpose of displaying the limits of the currently used formulas.
- (ii) The numerical approach is described and its reliability is verified by comparing its results with the analytical solutions of those situations (symmetrical Gouy-Chapmann case) for which the Poisson-equation of the SCL can be analytically solved without approximations.
- (iii) Subsequently, the numerical approach is used to map the conductivity variations also in those cases, for which the assumptions made for the Mott-Schottky and asymmetric Gouy-Chapman approximations are questionable (mixed situations and low SCL potentials).
- (iv) In the light of the results obtained with the numerical approach, a set of new, refined analytical solutions is proposed, which provide more accurate solutions of the space charge profiles.
- (v) Finally, 3 examples from the literature are considered and treated according to the approximated analytical solutions, the numerical approach as well as the improved analytical solutions.

1.1 Cerium oxide

As a case study we consider here cerium oxide (CeO_2), which is a prominent example of a material dominated by SCL effects.^{7, 9-18} Typically, undoped and acceptor-doped CeO_2 exhibit positive ϕ_0 values at the GBs ranging between 0.19 and 0.34 V.¹⁹⁻²⁴ This results in a depletion of the oxygen vacancies at the SCLs and an enrichment of the excess electrons. Depending on the experimental conditions (temperature and doping content), in nanocrystalline samples the total ionic conductivity was found to be varied by up to three orders of magnitude (compared with the bulk properties) leading to unusual phenomena such as a pronounced electronic contribution to the conductivity even for strongly acceptor doped samples at low temperatures and under oxidizing conditions.^{IV 23}

SCL effects in ceria are particularly interesting not only for basic research but also for applications such as solid oxide fuel cells,²⁵⁻²⁷ oxygen membranes²⁸⁻³² and catalysis.³³⁻³⁵ Notably, for the first two mentioned technologies it is the very high oxygen vacancy conductivity in acceptor doped ceria that is of highest importance. However, as mentioned above, due to the positively charged GB core, the overall ionic conductivity of polycrystalline ceria is limited. Therefore, a number of different approaches have been reported in the literature aimed at modifying the SCL properties. They include inhomogeneous doping by GB diffusion,³⁶ segregation of aliovalent cations at the boundaries,³⁷ decoration of the GBs of nanocrystalline ceria,^{38, 39} and use of substrates on which CeO_2 films with only small positive potentials can be grown.²⁴

Before addressing the SCL effects, it is worth briefly considering the bulk defect chemistry of CeO_2 , which (at low oxygen partial pressures $p\text{O}_2$) is affected by the reduction of cerium(IV) to cerium(III) upon formation of oxygen vacancies V_{O}^{\square} ^{40, 41}:



$$K = p\text{O}_2^{1/2} \cdot c_{V_{\text{O}}^{\square}, \infty} \cdot n_{\infty}^2 \quad \{9\}$$

$$K = K_0 \cdot e^{-\frac{\Delta H}{k_B T}} \quad \{10\}$$

$$2c_{V_{\text{O}}^{\square}, \infty} + c_{D^{\bullet}} = n_{\infty} + c_{A^{\prime}} \quad \{11\}$$

In equation {11} (electroneutrality condition), $c_{D^{\bullet}}$ and $c_{A^{\prime}}$ are donor and acceptor dopant concentrations with $|z|=1$, while n_{∞} is the electron concentration. It is important to note that the values of the approximately temperature independent parameters ΔH (oxygen excorporation enthalpy) and K_0 (the corresponding equilibrium constant of the law of mass action) in the literature

^{IV} 25% of the total conductivity is electronic for 10 mol% Gd doping at 280°C and $p\text{O}_2 = 10^{-5}$ bar.²²

vary depending on the investigated samples. This is the case particularly for ΔH , whose values reported in previous studies are considerably scattered.^{13, 20, 40, 42, 43} In the present contribution, for the electron bulk concentration, the experimental data obtained from epitaxial nominally pure CeO₂ layers studied in ref. 20 are considered, namely $n_{\infty} = 2 \cdot 10^{18} \text{ cm}^{-3}$, obtained at 700 °C and $p\text{O}_2 = 1 \text{ bar}$. The other relevant parameters used in the present study are listed in Table 2.^V Note that the case of nanocrystalline ceria is considered here ($d = 40 \text{ nm}$), for which the extent of the space charge layer is always smaller than the average grain size ($2\ell_{\text{SCL}} < d$, see also Fig. 3a in Part II).⁶ Moreover, the dopant is considered here as immobile.

Table 1 Definition of the physical quantities used in the present study. Note that in this contribution the subscript 0 generally denotes the coordinate $x = 0$, i.e. the position adjacent to the interface (e.g. ϕ_0 is the electric potential at the interface). The subscript ∞ denotes the bulk of the material. Furthermore, a prime ' denotes a preliminary, non-corrected quantity.

| Variables | Description |
|---|---|
| A | parameter in the GC case, see parameters section in Table 6 |
| $c_{A'}$ | acceptor dopant concentration ($z = -1$) |
| $c_{D'}$ | donor dopant concentration ($z = 1$) |
| $c_{\text{depl},\infty}$ | bulk concentration of the depleted charge carrier |
| $c_i, c_{i,x}$ | local concentration of mobile charge carrier i (at coordinate x) |
| $c_{i,\infty}$ | bulk concentration of mobile charge carrier i |
| $c_{\text{IM},j}$ | bulk concentration of immobile charge carrier j |
| $c_{\text{maj},\infty}$ | bulk concentration of the enriched majority charge carrier |
| $c_{\text{enr},\infty}$ | bulk concentration of the enriched minority charge carrier |
| $c_{\text{VO}^{\bullet\bullet}}$ | local oxygen vacancy concentration |
| $c_{\text{VO}^{\bullet\bullet},\infty}$ | oxygen vacancy bulk concentration |
| d | grain size |
| d_L | individual layer thickness |
| d_{TF} | thin film thickness |
| e | elementary charge ($1.60217648 \cdot 10^{-19} \text{ C}$) |
| E, E_x | electric field (at coordinate x) |
| i | counter variable for mobile charge carriers |
| j | counter variable for immobile charge carriers |
| k | counter variable for calculation steps |
| k_B | Boltzmann constant ($1.381 \cdot 10^{-23} \text{ J/K}$) |
| K | equilibrium constant of the CeO ₂ reduction reaction |

^V Note that in undoped ceria ($n_{\infty} \propto p\text{O}_2^{-1/6}$), the electron concentration $n_{\infty} = 2 \cdot 10^{18} \text{ cm}^{-3}$ (at $p\text{O}_2 = 1 \text{ bar}$) corresponds to $n_{\infty} = 9 \cdot 10^{19} \text{ cm}^{-3}$ at $p\text{O}_2 = 10^{-10} \text{ bar}$.

| | |
|------------------------------|--|
| K_0 | pre-exponential factor of the equilibrium constant |
| ℓ_{SCL} | combined length of the SCL |
| n | local electron concentration |
| n_∞ | electron bulk concentration |
| N_{IM} | number of immobile charge carriers |
| N_M | number of mobile charge carriers |
| pO_2 | oxygen partial pressure |
| $s_{e',m}$ | normalized conductivity of the electrons (including parallel and perpendicular boundary contributions) |
| $s_{i,m}$ | normalized conductivity of the charge carrier i (including parallel and perpendicular boundary contributions) |
| $s_{i,m}^{\parallel}$ | normalized conductivity of the charge carrier i in a sample only containing only parallel SCLs |
| $s_{i,m}^{\perp}$ | normalized conductivity of the charge carrier i in a sample only containing only perpendicular SCLs |
| $s_{i,m}^{Approx}$ | normalized conductivity of the charge carrier i calculated using an analytical approach |
| $s_{i,m}^{Num}$ | normalized conductivity of the charge carrier i calculated using the numerical approach |
| $s_{V_O^{\bullet\bullet},m}$ | normalized conductivity of the oxygen vacancies (including parallel and perpendicular boundary contributions) |
| T | temperature |
| x, x_k | distance from boundary (at calculation step k) |
| x_{MS} | distance corresponding to Σ_{SCL} / ρ_0 (see Table 6) |
| z_{depl} | charge number of the depleted charge carrier |
| $z_{e'}$ | charge number of the electrons ($z_{e'} = -1$) |
| z_i | charge number of mobile charge carrier i |
| $z_{IM,j}$ | charge number of immobile charge carrier j |
| z_{enr} | charge number of the enriched minority charge carrier |
| z_{maj} | charge number of the enriched majority charge carrier |
| $z_{V_O^{\bullet\bullet}}$ | charge number of the oxygen vacancies ($z_{V_O^{\bullet\bullet}} = +2$) |
| I^{\parallel} | one-dimensional density of the parallel SCLs (see Table 3) |
| I^{\perp} | one-dimensional density of the perpendicular SCLs (see Table 3) |
| δ_i | deviation between the outcome (normalized conductivity value) of an analytical approach and the numerical calculations |
| ΔH | reduction enthalpy |
| Δs_i^{\parallel} | normalized conductivity change of the charge carrier i due to the parallel SCLs |
| Δx_k | length interval (at calculation step k) |
| $\Delta \rho$ | (3-dimensional) charge density difference |
| $\Delta \Sigma_{i,GC}$ | contribution of the GC-like part of the profile on Σ_i in the mixed case (Table 6) |
| $\Delta \Sigma_{i,MS}$ | contribution of the MS-like part of the profile on Σ_i in the mixed case (Table 6) |
| $\Delta \Omega_{i,GC}$ | contribution of the GC-like part of the profile on Ω_i in the mixed case (Table 6) |
| $\Delta \Omega_{i,MS}$ | contribution of the MS-like part of the profile on Ω_i in the mixed case (Table 6) |
| θ | temperature in °C |
| ϑ_i | influence factor in the symmetrical GC case |
| λ | Debye length |

| | |
|----------------------------|---|
| λ^* | screening length (Mott-Schottky case) |
| $\lambda_{e'}$ | Debye length (concerning e' bulk concentration) |
| $\lambda_{V_O^{**}}$ | Debye length (concerning V_O^{**} bulk concentration) |
| ε_0 | vacuum permittivity ($8.854 \cdot 10^{-12}$ F/m) |
| ε_r | relative permittivity |
| ρ, ρ_x | (3-dimensional) charge density (at coordinate x) |
| ρ_{IM} | charge density contribution of immobile charge carriers |
| $\sigma_{e',m}$ | absolute conductivity of the electrons (including parallel and perpendicular boundary contributions) |
| $\sigma_{e',\infty}$ | bulk conductivity of the electrons |
| $\sigma_{i,m}$ | total effectively measured conductivity of charge carrier i (including parallel and perpendicular boundary contributions) |
| $\sigma_{i,\infty}$ | bulk conductivity of charge carrier i |
| $\sigma_{V_O^{**},m}$ | absolute conductivity of the oxygen vacancies (including parallel and perpendicular boundary contributions) |
| $\sigma_{V_O^{**},\infty}$ | bulk conductivity of the oxygen vacancies |
| Σ_{Core} | grain boundary core charge |
| Σ_i | charge contribution due to the enrichment (or depletion) of mobile charge carrier i |
| Σ_{SCL} | charge of the SCL |
| Φ, Φ_x | electric potential (at coordinate x) |
| Φ_T | transition potential in the mixed case |
| Ω_i | reduced resistance change of the SCL in perpendicular direction concerning the transport of mobile charge carrier i |

Table 2 Values of the parameters used in the present study.

| | |
|-----------------|-----------------------------------|
| n_∞ | $2 \cdot 10^{18} \text{ cm}^{-3}$ |
| θ | 700°C |
| pO_2 | 10^{-10} bar |
| ε_r | 26 |
| d | 40 nm |

1.2 Analytical solutions of the Poisson-equation

It is worth noting that in the vast majority of contributions dealing with SCL effects in ionic and mixed conductors analytical approximations have been employed.^{1, 2, 44} Remarkably, the Poisson-equation of the SCL profile can be solved analytically only for the “symmetrical” Gouy-Chapman situation of two intrinsic charge carriers 1 and 2 with $z_1 = -z_2$. For all the other cases (which are actually present in CeO₂ with $z_{e^-} = -1$ and $z_{V_{O^{\bullet\bullet}}} = +2$) certain approximations are available.⁴⁴ They rely on the strong enrichment (or depletion) of only one charge carrier, while the influence of the counter-charge carrier is entirely neglected. For this reason, the analytical approximations can only describe the ideal Gouy-Chapman and Mott-Schottky situations for large effects but neither for mixed cases nor weak effects (low potentials). In the following, the main analytical results regarding the space charge potential profile are summarized.^{2, 45} Further details on the relationships can be found in the Supplementary Information.^{1, 2, 44}

$$\text{MS case: } \Phi = -\frac{z_{IM}e c_{IM}}{2\varepsilon_r \varepsilon_0} (x - \lambda^*)^2, \quad \lambda^* = \sqrt{-\frac{2\varepsilon_r \varepsilon_0 \Phi_0}{z_{IM}e c_{IM}}}, \quad x < \lambda^* \quad \{12\}$$

$$\text{GC case: } \Phi = \Phi_0 + \frac{2k_B T}{z_{maj} e} \ln \left(1 + \frac{x}{2\lambda} e^{\frac{z_{maj} e}{2k_B T} \Phi_0} \right), \quad \lambda = \sqrt{\frac{\varepsilon_r \varepsilon_0 k_B T}{2z_{maj}^2 e^2 c_{maj, \infty}}}, \quad x < 2\lambda \quad \{13\}$$

$$\text{symmetrical GC case: } \Phi = -\frac{2k_B T}{z_i e} \ln \left(\frac{1 + g_i \cdot e^{-\frac{x}{\lambda}}}{1 - g_i \cdot e^{-\frac{x}{\lambda}}} \right), \quad g_i = \frac{e^{-\frac{z_i e}{2k_B T} \Phi_0} - 1}{e^{-\frac{z_i e}{2k_B T} \Phi_0} + 1}, \quad \{14\}$$

where λ^* is the Mott-Schottky length and λ the Debye length, while $c_{maj, \infty}$ and z_{maj} are the bulk concentration of the majority charge carrier and its corresponding charge number, respectively. If the above relationships are inserted in eq. {2} the SCL concentration profiles are obtained. The integration of the concentration profile of a mobile defect i yields its charge contribution Σ_i to the total SCL charge Σ_{SCL} :

$$\Sigma_i = z_i e \cdot \int_0^{\infty} (c_i - c_{i, \infty}) dx. \quad \{15\}^{VI}$$

^{VI} The upper integration limit is different for the GC and MS cases. For details see the Supplementary Information.

In a similar manner, in the case of a depletion of the charge carrier i , the normalized electrical resistance across the SCLs Ω_i (aligned perpendicularly to the transport direction) can be defined:

$$\Omega_i \equiv \frac{1}{|z_i|e} \cdot \int_0^{\infty} (c_i^{-1} - c_{i,\infty}^{-1}) dx. \quad \{16\}$$

Obviously, a change the mobile charge carrier concentrations within the SCLs, results in a conductivity change compared with the bulk situation, which can be expressed as

$$s_{i,m} = \frac{\sigma_{i,m}}{\sigma_{i,\infty}}, \quad \{17\}$$

with $\sigma_{i,m}$ being the total effectively measured conductivity of the charge carrier i (including the influence of both parallel and perpendicular SCLs) and $\sigma_{i,\infty}$ its corresponding bulk conductivity. Here, it is convenient to treat the material microstructure according to the brick layer model^{1, 46} (cubically shaped grains having here size d), which allows for estimating the effect of the non-overlapping SCLs on the conductivity of a polycrystalline material. In the case of an enrichment of charge carriers the SCLs which are aligned parallel to the direction of electric transport are of relevance and the following relationship results:

$$\text{Enriched charge carrier: } s_{i,m} = s_{i,m}^{\parallel} \quad \text{with} \quad s_{i,m}^{\parallel} = \Gamma^{\parallel} \cdot \frac{\Sigma_i}{z_i e c_{i,\infty}} + 1. \quad \{18\}$$

In the case of depletion, the perpendicular boundaries are crucial and one can write:

$$\text{Depleted charge carrier: } s_{i,m} = s_{i,m}^{\perp} \quad \text{with} \quad s_{i,m}^{\perp} = \left(\Gamma^{\perp} |z_i| e c_{i,\infty} \Omega_i + 1 \right)^{-1}. \quad \{19\}$$

Here, in the brick layer model Γ^{\parallel} and Γ^{\perp} are the one-dimensional densities of the parallel and perpendicular SCLs, respectively. They are given in **Table 3** for several sample geometries.

Table 3 One-dimensional densities of the parallel and perpendicular SCLs Γ^{\parallel} and Γ^{\perp} for different, relevant experimental situations

| Geometry | Γ^{\parallel} | Γ^{\perp} |
|--|----------------------|------------------|
| pellet | $\frac{4}{d}$ | $\frac{2}{d}$ |
| thin film with polycrystalline, columnar structure, measurement parallel to the substrate | $\frac{2}{d}$ | $\frac{2}{d}$ |
| thin film with polycrystalline, columnar structure, measurement perpendicular to the substrate | $\frac{4}{d}$ | 0 |
| thin film with epitaxial multilayers, measurement parallel to the substrate | $\frac{2}{d_L}$ | 0 |
| thin film with epitaxial multilayers, measurement perpendicular to the substrate | 0 | $\frac{2}{d_L}$ |
| epitaxial thin film with SCL at the film substrate interface (or at the film surface), measurement parallel to the substrate | $\frac{1}{d_{TF}}$ | 0 |

As far as the SCL profiles in ceria are concerned, 8 different cases depending on doping content and ϕ_0 can be identified, as illustrated in **Fig. 2**: Here the designations of ref. 43, where the analytical solutions are compiled, are used for clarity. The relevant formulas (derived using the models described above) and concentration profiles are given in **Table 4**. The variations of the normalized oxygen vacancy conductivity $s_{V_{O^{\bullet\bullet}},m} = \sigma_{V_{O^{\bullet\bullet}},m} / \sigma_{V_{O^{\bullet\bullet}},\infty}$ (i.e. effectively measured ionic conductivity over bulk ionic conductivity) obtained analytically are plotted in the left contour plot of **Fig. 3** as a function of a broad range of dopant concentrations and $|\phi_0|$ values (cf. also footnote II). The resulting conductivity change (z-axis) is color-coded. For clarity, the bulk concentrations are plotted in **Fig. 4** (note that for the donor doped situation, only the case expected for $pO_2 = 10^{-10}$ bar and $c_D = n$, is considered – see also ref. 18). Experimentally, only pure and acceptor doped ceria have been extensively investigated in terms of SCL effects with ϕ_0 values ranging between 0.19 and 0.34 V¹⁹⁻²⁴, as indicated by the blue rectangle in **Fig. 3**.

As mentioned above, there are a number of studies, which have addressed the possibility of adjusting ϕ_0 with the purpose of improving the GB conduction properties. For this reason, a wider range of ϕ_0 (including even $\phi_0 < 0$) was considered here, in order to predict the possible outcome of such adjustments.^{vii} A detailed description of this kind of contour plot is given in Section 2.1. Here it

^{vii} Note that for some situations SCL profiles with very large potentials cannot be realized since in these cases the charge of the SCL becomes unrealistically large. These situations and a detailed discussion of the role of the SCL charge are given in Part II of this contribution (in Section 2.2).

is sufficient to focus on only one particular aspect, which is indicated by the crossed area in **Fig. 3**: Notably, for $|\Phi_0| < 0.2$ V (for the oxygen vacancies, left panel of **Fig. 3**) the approximations yield wrong conductivities: e.g. the approximations give $s_{V_O^{\bullet\bullet},m} < 1$ (indicating depletion) for negative potentials whereas $V_O^{\bullet\bullet}$ are enriched, and $s_{V_O^{\bullet\bullet},m} > 1$ (indicating enrichment) for positive potentials which instead are characterized by a depletion of $V_O^{\bullet\bullet}$. This effect is even more pronounced for the electrons due to their smaller charge (see the right panel).

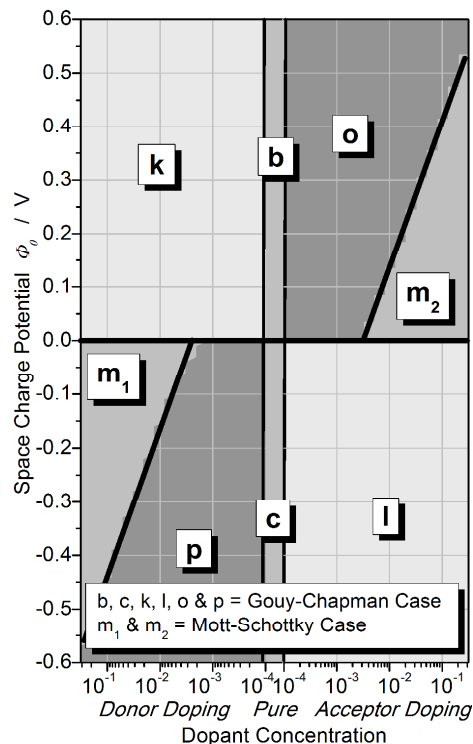
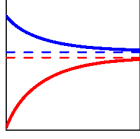
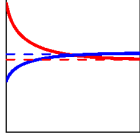
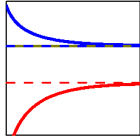
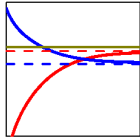
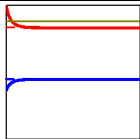
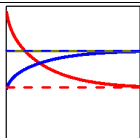
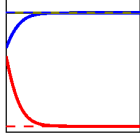
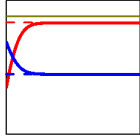


Fig. 2 Map of the different analytical approximations given in **Table 4** as a function of the dopant concentration and ϕ_0 (designations according to ref. 43). In order to define the border between the GC and the MS cases, the concentration of the enriched charge carrier at the interface is compared with the dopant concentration: For positive ϕ_0 and acceptor doping the MS case was applied if the electron concentration at the interface $n_0 = n_\infty \exp(e\phi_0 / k_B T)$ is smaller than the dopant concentration c_A . Similarly for negative potentials and donor doping the criterion $c_{V_O^{\bullet\bullet},0} = c_{V_O^{\bullet\bullet},\infty} \exp(-2e\phi_0 / k_B T) < c_D$ was used to border the MS case.

Table 4 Approximative solutions of the SCL conductivity effects given in ref. 43.

| Case | Type | Example Profile | Condition | $s_{V_{O^{\bullet\bullet}},m} = \frac{\sigma_{V_{O^{\bullet\bullet}},m}}{\sigma_{V_{O^{\bullet\bullet}},\infty}}$ | $s_{e',m} = \frac{\sigma_{e',m}}{\sigma_{e',\infty}}$ |
|--|---------------|---|--------------------------------------|---|---|
| <i>b</i> | Gouy-Chapman |  | | $\frac{d}{4\lambda_{V_{O^{\bullet\bullet}}}^{\bullet\bullet}} \cdot e^{\frac{-3/2 e\phi_0}{k_B T}}$ | $\frac{8\lambda_{e'} \cdot e^{\frac{1/2 e\phi_0}{k_B T}}}{d}$ |
| <i>c</i> | |  | | $\frac{8\lambda_{V_{O^{\bullet\bullet}}}^{\bullet\bullet}}{d} \cdot e^{\frac{-e\phi_0}{k_B T}}$ | $\frac{d}{4\lambda_{e'}} \cdot \frac{k_B T}{-e\phi_0}$ |
| <i>k</i> | |  | | $\frac{d}{4\lambda_{V_{O^{\bullet\bullet}}}^{\bullet\bullet}} \cdot \sqrt{n_\infty} \cdot e^{\frac{-3/2 e\phi_0}{k_B T}}$ | $\frac{8\lambda_{e'} \cdot e^{\frac{1/2 e\phi_0}{k_B T}}}{d}$ |
| <i>o</i> | |  | $n_0 > c_A$ | | $\frac{d}{4\lambda_{e'}} \cdot \sqrt{\frac{c_{V_{O^{\bullet\bullet}},\infty}}{n_\infty}} \cdot \frac{k_B T}{-e\phi_0}$ |
| <i>l</i> | |  | | | |
| <i>p</i> | |  | $c_{V_{O^{\bullet\bullet}},0} > c_D$ | | |
| <i>m₁</i> | Mott-Schottky |  | $c_{V_{O^{\bullet\bullet}},0} < c_D$ | $\frac{2\lambda_{e'}}{d} \cdot \frac{e^{\frac{-2e\phi_0}{k_B T}}}{\sqrt{\frac{-e\phi_0}{k_B T}}}$ | $\frac{d}{2\lambda_{e'}} \cdot \frac{\sqrt{\frac{-e\phi_0}{k_B T}}}{e^{\frac{-e\phi_0}{k_B T}}}$ |
| <i>m₂</i> | |  | $n_0 < c_A$ | $\frac{d}{2\lambda_{V_{O^{\bullet\bullet}}}^{\bullet\bullet}} \cdot \frac{\sqrt{\frac{2e\phi_0}{k_B T}}}{e^{\frac{2e\phi_0}{k_B T}}}$ | $\frac{4\lambda_{V_{O^{\bullet\bullet}}}^{\bullet\bullet}}{d} \cdot \frac{e^{\frac{e\phi_0}{k_B T}}}{\sqrt{\frac{1/2 e\phi_0}{k_B T}}}$ |
| <p>— $V_{O^{\bullet\bullet}}$ — e' — Dopant — — $V_{O^{\bullet\bullet}}$ (bulk) — — e' (bulk)</p> <p>$\lambda_{V_{O^{\bullet\bullet}}}^{\bullet\bullet} = \sqrt{\frac{\epsilon_r \epsilon_0 k_B T}{8e^2 c_{V_{O^{\bullet\bullet}},\infty}}}, \quad \lambda_{e'} = \sqrt{\frac{\epsilon_r \epsilon_0 k_B T}{2e^2 n_\infty}}$</p> | | | | | |

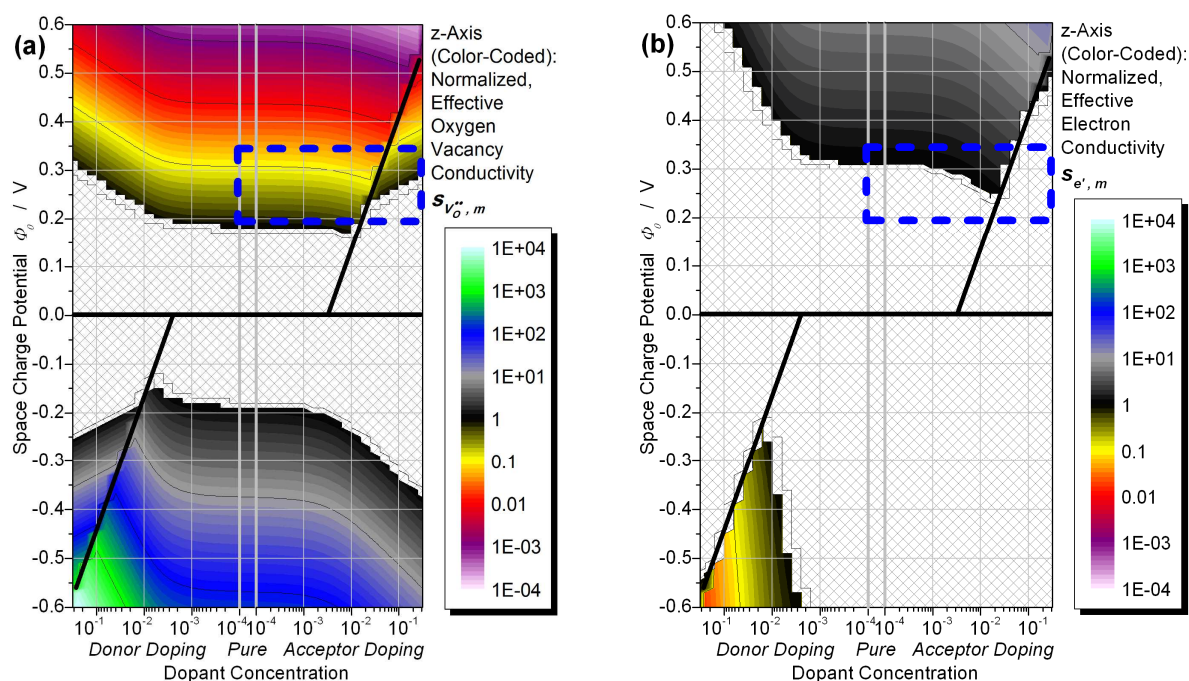


Fig. 3 Normalized effective conductivities $s_m = \sigma_m / \sigma_\infty$ of (a) oxygen vacancies and (b) electrons calculated using the analytical approximations given in **Table 4** in a polycrystalline CeO_2 pellet with $d = 40$ nm as function of doping content and SCL potential. The crossed areas indicate positions where the relationships produce non-physical results (i.e. depletion in case of enrichment and vice versa). The blue dashed rectangle indicates the range of characteristic values of dopant concentration and ϕ_0 determined experimentally in the literature for CeO_2 .¹⁹⁻²⁴ The s_m values plotted along the z-axis are color-coded. The black areas correspond to $s_m \approx 1$ ($\sigma_m \approx \sigma_\infty$), indicating no or only very small SCL effects. For the oxygen vacancies, s_m decreases when $\phi_0 > 0$. The corresponding s_m drop is depicted by the yellow, red and purple colors, which correspond to $\sigma_m \approx 0.1 \sigma_\infty$, $\sigma_m \approx 0.01 \sigma_\infty$ and $\sigma_m \approx 0.001 \sigma_\infty$, respectively. For $\phi_0 < 0$, the effective ionic conductivity is expected to increase. The corresponding color-coding is here grey ($\sigma_m \approx 10 \sigma_\infty$), blue ($\sigma_m \approx 100 \sigma_\infty$) and green ($\sigma_m \approx 1000 \sigma_\infty$). The SCL effects in the case of the electrons are more moderate due to $|z_e| = 1$. Note that a more comprehensive discussion of the here displayed SCL conductivity effects is given in Section 2.1 and in Part II of this study.⁶

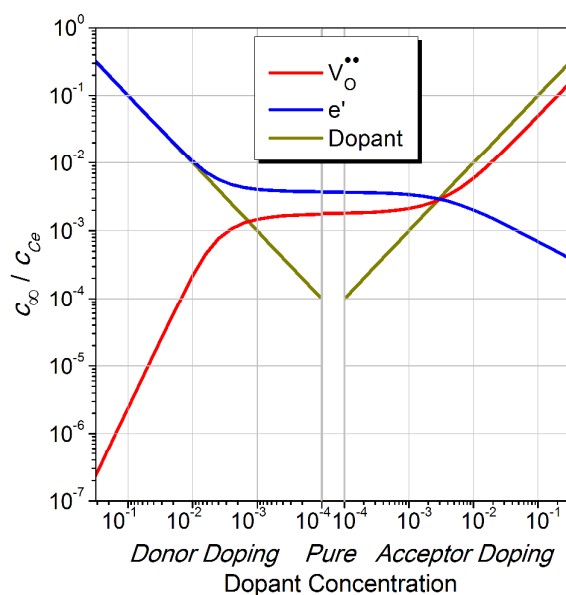


Fig. 4 Bulk concentrations $c_{V_O^{..}, \infty}$ and n_{∞} as a function of doping content $c_{D'}$ and $c_{A'}$, calculated using the parameters of Table 2.

The origin of these obvious discrepancies is the fact that the total effective conductivity in ref. 43 and **Table 4** is set to be equal to the conductivity change (e.g. $s_i^{\parallel} = \Delta s_i^{\parallel} + 1 \approx \Delta s_i^{\parallel}$). In order to avoid this uncertainty the terms in **Table 4** have to be set equal to $s_{i,m} - 1$ in the case of enrichment and $(s_{i,m}^{-1} - 1)^{-1}$ in the case of depletion. The improvements upon this rather straightforward correction are graphically illustrated in **Fig. 5**.

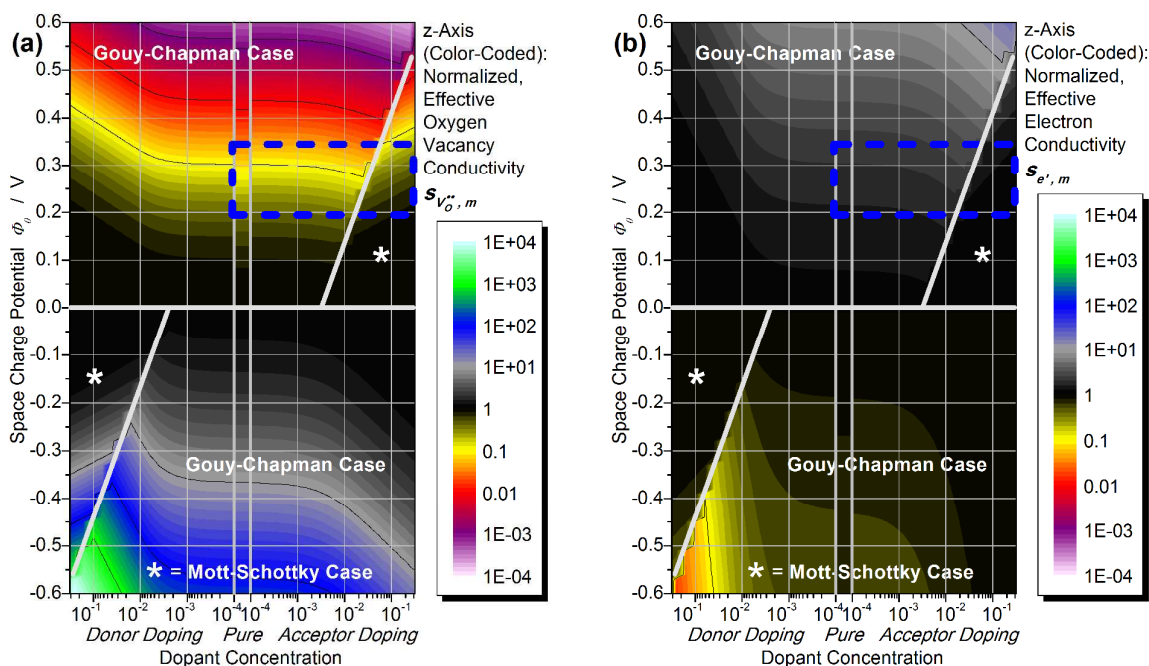


Fig. 5 Normalized conductivity of (a) oxygen vacancies and (b) electrons obtained using the analytical solutions in **Table 4** and taking into account the bulk conductivity contribution (see main text). Note that a detailed explanation of the color-coding is given in the caption of **Fig. 3**.

Here it is instructive to consider once again that the analytical solutions are derived under the assumption of strong effects (large potentials). Obviously, for small potentials this assumption does not hold. Here, one should also note that, as illustrated in **Fig. 3**, the region of small potentials is not negligibly small. For cerium oxide, it clearly extends into the range of experimentally determined SCL potentials, which spans between 0.19 and 0.34 V¹⁹⁻²⁴ (see the blue rectangle in **Fig. 3** and **Fig. 5**).

Therefore, also the further simplifications, which rely on the assumption of a strong effect (e.g. the fact that in the Gouy-Chapman case only the enriched charge carrier is considered) are questionable at potential values being experimentally relevant. These considerations made a systematic analysis of the accuracy of the analytical solutions by means of a numerical approach particularly interesting.

2 Numerical Method

This section gives a brief overview of the numerical approach used here. The details and definitions of the related quantities are elucidated in the Supplementary Information. It is worth stressing here that this study deals with the effects of non-overlapping SCLs as schematically depicted in **Fig. 1**.

The algorithm to numerically solve the Poisson-equation is based on a stepwise calculation of the electrical potential ϕ using a Taylor expansion of degree three:

$$\Phi_{x_k} \approx \Phi_{x_{k-1}} - \Delta x_k \cdot E_{x_{k-1}} - \frac{\Delta x_k^2}{2\varepsilon_r \varepsilon_0} \left(\rho_{x_{k-1}} + \frac{\Delta \rho}{3} \right) \quad \{20\}$$

Note that $x_k = x_{k-1} + \Delta x_k$. The calculation step k ranges from 1 to N_{steps} (cf. the Supplementary Information). The electrical field E , the charge density ρ and the defect concentrations c_i can be determined using the following relationship⁴⁷

$$E_{x_k} = \text{sgn}(\Phi_{x_k}) \cdot \sqrt{\frac{2k_B T}{\varepsilon_r \varepsilon_0} \left(\sum_{i=1}^{N_M} (c_{i,x_k} - c_{i,\infty}) - \frac{\rho_{IM}}{k_B T} \Phi_{x_k} \right)} \quad \{21\}$$

and taking into account eq. {2}, {3} and {5}. Notably, in addition to the material properties (e.g. dopant concentration) and the experimental conditions (e.g. T and pO_2), Φ_0 is used here as input parameter for the calculation. The profiles obtained in this way were tested for the “symmetrical GC case” (two intrinsic charge carriers 1, 2 with $z_1 = -z_2$), for which the exact analytical solution is available without any approximation.² As shown in the Supplementary Information (Section S3), the relative differences were found to be extremely small, namely in the range between 10^{-10} % and 0.1 % even for extremely steep profiles with very high potentials. In order to determine SCL effects on the conductivity, the brick layer model described in Section 1.2 was applied, i.e. eq. {17} to {19} (the integration of the concentration profiles was performed numerically).

2.1 Conductivity maps

Fig. 6 shows the effect of the space charge properties on the overall conductivity of the oxygen vacancies (left panel) and electrons (right panel) calculated according to the numerical method illustrated above. As expected for potentials close to zero the conductivity change is only small as indicated by the black area. For $\Phi_0 > 0$, the oxygen vacancies are depleted and the perpendicular GBs block the ionic transport, whereas for $\Phi_0 < 0$ the $V_O^{\bullet\bullet}$ enrichment at the parallel GBs leads to a conductivity increase. Clearly, with rising absolute values of Φ_0 , the blocking (or short-circuiting) effect of the SCLs increases (see the yellow, red and purple areas (conductivity decrease) and the grey, blue and green areas (conductivity increase) in the left panel of **Fig. 6**). The maximum conductivity enhancement (or depression) amounts up to 3 orders of magnitude compared with the bulk properties (for the given parameters). For the electrons (enriched for positive and depleted for negative potentials) the conductivity changes are qualitatively similar but much less pronounced due to their lower valence (see eq. {2}). In addition, it is worth noting that the variations of σ_m with

respect to σ_∞ do not only depend on Φ_0 but also on the dopant content. Notably, for a given potential, the conductivity change becomes smaller when the dopant concentration increases (i.e. s_m approaches unity).

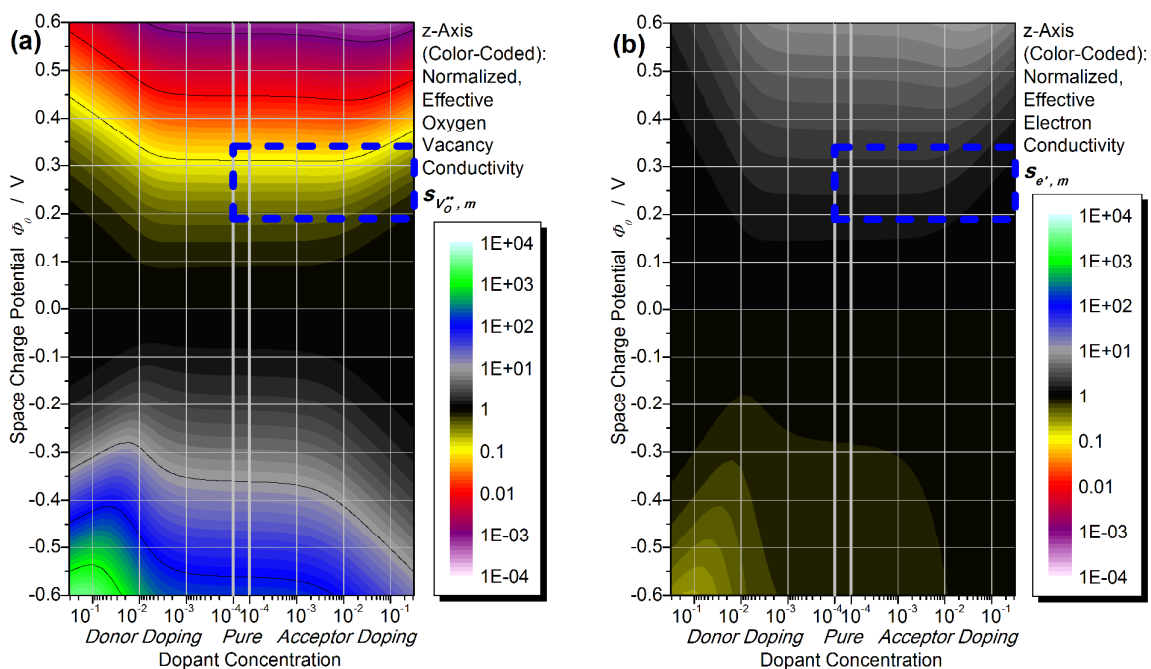


Fig. 6 Normalized effective conductivity $s_m = \sigma_m / \sigma_\infty$ of (a) oxygen vacancies and (b) electrons calculated using the numerical approach. Note that a detailed explanation of the color-coding is given in the description of Fig. 3.

3 Analytical approximations vs numerical solutions

At this point, it is instructive to quantitatively compare the analytical approximations with the numerical solutions using the deviation values δ (**Fig. 7**), which are defined as follows:

$$\text{in the case of enrichment of the charge carrier } i: \quad \delta_i = \frac{s_{i,m}^{Approx} - 1}{s_{i,m}^{Num} - 1} \quad \{22\}$$

$$\text{in the case of depletion of the charge carrier } i: \quad \delta_i = \frac{(s_{i,m}^{Approx})^{-1} - 1}{(s_{i,m}^{Num})^{-1} - 1}. \quad \{23\}$$

Here, $s_{i,m}^{Approx}$ results from the analytical approximations (including the correction given at the end of Section 1.2 by setting $s_{i,m} - 1$ or $(s_{i,m}^{-1} - 1)^{-1}$ – see also **Fig. 5**), while $s_{i,m}^{Num}$ are the numerical results. Depending on the values of δ_i , it is possible to verify whether the analytical approximations correctly estimate ($\delta_i = 1$), underestimate ($\delta_i < 1$) or overestimate ($\delta_i > 1$) the change of $s_{i,m}$. For example, an increase of the conductivity (compared with the bulk) of 5% obtained with the numerical approach and an increase of 10% obtained using the analytical approximations results in a deviance value of 2 (calculated according to eq. {22}).

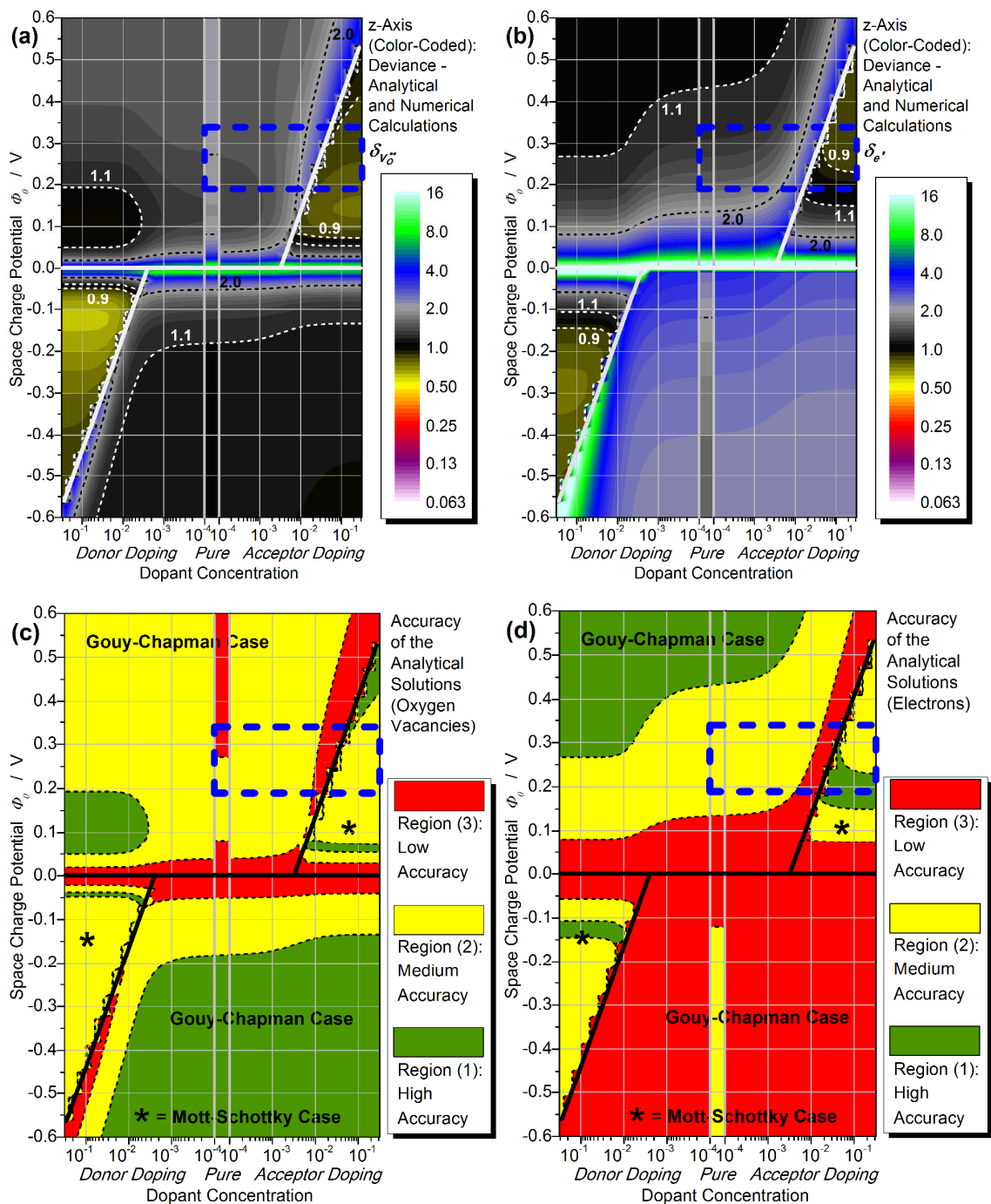


Fig. 7 Panels (a) and (b): deviance δ_i between the analytical⁴³ (upon having taken into account the bulk conductivity – cf. **Fig. 5**) and the numerical solutions calculated as a function of dopant concentration and ϕ_0 for oxygen vacancies and electrons, respectively. The black regions ($\delta_i = 1$) indicate that both approaches yield identical results. If $\delta_i < 1$ ($\delta_i > 1$), the analytical approach underestimates (overestimates) the effective conductivity change. In (c) and (d) maps of accuracy defined according to the deviance value are plotted for oxygen vacancies and electrons, respectively.

The deviance values can be used to define regions of different accuracy as depicted in green, yellow and red in **Fig. 7c** and **Fig. 7d**.

- The green region (1) corresponds to the analytical approximations being very precise and exhibiting a difference of less than 10 % compared with the numerical approach ($0.9 < \delta_i < 1.1$).
- In the yellow region (2), $0.5 < \delta_i < 2.0$ holds, meaning that the analytical approximations deviate by up to a factor of 2 from the numerical calculations. Although at a first glance these deviations seem to be rather large, they are still acceptable if one considers that other simplifications contribute to a systematic error of similar magnitude (e.g. those concerning the geometry of the grains, i.e. the brick layer model).
- Finally, the red region (3) corresponds to deviations exceeding a factor of 2 ($\delta_i < 0.5$ or $\delta_i > 2.0$). Clearly, here the analytical approach is rather limited and should not be employed to estimate the conductivity changes.

These accuracy maps shown in **Fig. 7c** and **Fig. 7d** are useful to illustrate under which conditions the formulas of **Table 4** yield precise outcomes or, on the contrary, unreliable results. It is worth noting that the range of dopant concentration and potential values, in which the reliability of the analytical approximations is limited, is rather large. Furthermore, it includes values of ϕ_0 and c_A that have been often encountered experimentally (see the blue rectangle in **Fig. 7c** and **Fig. 7d**).

The reasons why the analytical approach gives - in certain situations - undependable outcomes are summarized in the following (see also Section 4.1).

(1) First, the equations listed in **Table 4** are obtained under the assumption of a strong enrichment (or depletion) effect. It is, therefore, obvious that the accuracy of such solutions is particularly limited when the term $|z_i| e\phi_0/k_B T$ is small (see eq. {2}), e.g. for low values of ϕ_0 and/or high temperatures (see **Fig. 7**). Note also that, due to the same reason, for the electrons ($|z_e|=1$) the accuracy region (1) is smaller while region (3) is larger compared to the oxygen vacancy case ($|z_{V_O^{\bullet\bullet}}|=2$). As discussed in Section 4.1, the neglect of the further constant (potential independent) terms in the derivation of the formulas shown in **Table 4** can yield particularly large errors, where the term $z_i e\phi_0/k_B T$ is not in the exponent (compare the cases c, l and p for the electrons in **Table 4** and **Fig. 2** with the extended red area at negative potentials in **Fig. 7d**).

(2) The second reason is related to the misleading assumption that the mixed case can be treated as the GC case. One should note that, in the mixed case, despite its low bulk concentration, the minority charge carrier is enriched above the much higher dopant concentration level (i.e. cases o and p in **Table 4** and **Fig. 2**), while, in the GC case, it is the majority charge carrier which is enriched (cases b, c, k and l in **Table 4** and **Fig. 2**). Such discrepancy causes large inaccuracies in proximity of the transition zones between the MS and GC situations (see **Fig. 7**). In the light of these considerations,

and since analytical approximations (**Table 4**)^{VIII} have been extensively used in the literature, we propose here new analytical solutions which can provide more satisfactory solutions of the space charge layer profiles.

4 New analytical solutions

4.1 Gouy-Chapman Case

For the GC case, the reduced accuracy results from the fact that the corresponding analytical solutions given in **Table 4** rely on the potential function obtained for the symmetrical GC case (see Section 1.2). This case, however, does not apply in a number of mixed and ionic conductors (such as CeO₂), as the condition $z_1 = -z_2$ does not hold.⁴⁴ In the following, it is shown that two modifications can significantly improve the accuracy of the analytical approach:

(1) Let us start with recalling that the formulas summarized in **Table 4** (derived under the assumption of strong SCL effects) are obtained neglecting the constant contributions to the space charge profiles, namely $e^{|e\phi_0/k_B T|} + const$ is set equal to $e^{|e\phi_0/k_B T|}$.⁴⁴ Obviously, to enhance the accuracy of the solutions, this approximation should be avoided. This is particularly important for those cases, in which the SCL profiles do not depend exponentially on ϕ_0 (e.g. the electronic conductivity in cases c, l and p in **Table 4**). If the analytical relationships of the GC case are derived without ignoring the constant contributions, eq. {31} and {33}–{38} in **Table 6** are obtained, which as expected are found to yield more precise outcomes.

(2) Let us now consider the outcomes of eq. {31} and {33}–{38}, i.e. the Σ'_i and Ω'_i values, as preliminary (denoted here by the prime superscript). The second modification concerns the fact that the derivation of these relationships relies on the potential profile $\phi(x)$ of the symmetrical GC situation. For non-symmetrical situations (e.g. for CeO₂), which cannot be solved analytically, this results in an over- or underestimation of the potential profile and, hence, in an over- or underestimation of the Σ'_i and Ω'_i values. Here it is instructive to consider a rather general property of SCLs. If the potential profile is overestimated (or underestimated) the degree of the resulting overestimation (underestimation) of the Σ'_i values of the enriched charge carriers and of the Ω'_i values of the depleted charge carriers is comparable. Since in the GC case the majority charge carrier (which contributes most to the SCL charge) is enriched and not depleted also Σ'_{SCL} is

^{VIII} or similar ones, depending on the charge numbers

overestimated (or underestimated) by approximately the same degree as the Σ'_i values and the Ω'_i values.^{ix} Hereby Σ'_{SCL} is the preliminary total SCL charge; i.e. the sum of all Σ'_i values.

However, as the real total SCL charge Σ_{SCL} can be analytically calculated without the use of further approximations (see eq. {4}), the degree of over- or underestimation can be evaluated easily by comparing Σ'_{SCL} with Σ_{SCL} . In the case of significant differences, the values of Σ'_i and Ω'_i can be corrected by using the factor $\Sigma_{SCL}/\Sigma'_{SCL}$. This yields the final quantities Σ_i and Ω_i (see eq. {30} in **Table 6**). Furthermore, if only the enriched majority charge carrier contributes significantly to Σ'_{SCL} , then eq. {31} simply becomes $\Sigma_{maj} = \Sigma_{SCL}$ (eq. {32}). The correction considerably improves the preciseness of the analytical approach even for low values of Φ_0 .

4.2 Mott-Schottky Case

Low Space Charge Potentials

Let us now consider the case of a conducting material having an enriched charge carrier 1 and an immobile charge carrier 2 (for simplicity $z_1 = -z_2$ and $c_{1,\infty} = c_{2,\infty}$). This corresponds to a GC case with

$$\rho = z_1 e c_{1,\infty} \cdot e^{-z_1 e \Phi_0 / k_B T} + z_2 e c_{2,\infty} = z_1 e c_{1,\infty} \cdot (e^{-z_1 e \Phi_0 / k_B T} - 1). \quad \text{For low } z_1 e \Phi_0 / k_B T \text{ values,}$$

$$e^{-z_1 e \Phi_0 / k_B T} \approx 1 - z_1 e \Phi_0 / k_B T \text{ and thus } \rho \approx z_1 e c_{1,\infty} \cdot (-z_1 e \Phi_0 / k_B T).$$

In a reverse situation (the charge carrier 1 is immobile and 2 is mobile and depleted), the MS case applies, for which $\rho = z_1 e c_{1,\infty} + z_2 e c_{2,\infty} e^{-z_2 e \Phi_0 / k_B T} = z_1 e c_{1,\infty} \cdot (1 - e^{z_1 e \Phi_0 / k_B T})$ holds. For low $z_1 e \Phi_0 / k_B T$ values, it follows that $\rho \approx z_1 e c_{1,\infty} \cdot (-z_1 e \Phi_0 / k_B T)$, which is exactly the same relationship derived above for the GC case. This means that, as long as only low $|\Phi_0|$ values and/or high temperatures are considered, the conductivity effects in the MS case can be treated in good approximation using the same relationships of the GC case (i.e. eq. {33}–{38} including the above described correction eq. {30}, see **Table 6** for further details). Notably, the numerical calculations showed that this analytical solution yields very precise conductivity values for $e^{|\Phi_0|/k_B T} < 4$.

^{ix} This is not the case if the MS case applies (unless the SCL potential is only low). Here for moderate and high potentials the majority charge carrier is strongly depleted. Therefore, an overestimation (underestimation) of the potential profile will result in an only very slight overestimation (underestimation) its Σ_i value and of the total SCL charge. In marked contrast, the resulting overestimation (underestimation) of its Ω'_i value will be very pronounced.

Moderate and Large Space Charge Potentials

The MS assumption of a constant charge density determined only by the immobile dopant results in a parabola profile of $\Phi(x)$ as shown in eq. {12} (see also the Supplementary Information). However, the expressions of the analytical solutions for the MS case available in literature (cases m_1 and m_2 in **Table 4**) rely on a further simplification, namely on the linearization of the potential profile:

$$\Phi = \Phi_0(1 - x/\lambda^*) \quad \{24\}$$

More precise relationships are expected if the more realistic $\Phi(x)$ parabola profile of eq. {12} is used instead. It is worth noting that the integration of the resulting e^{-x^2} terms from 0 to λ^* yields the analytical, non-elementary inverse error function erfi , which is closely related to the error function erf .^x Rather surprisingly, the so-obtained relationships (see **Table 5**) yield less precise conductivity values compared with the expressions obtained by using the linear potential profile.

Table 5 Relationships obtained considering the parabolic profile of the space charge potential in eq. {12}. Γ^{\parallel} and Γ^{\perp} are defined in **Table 3**. The Debye lengths are given in **Table 4**.

| | |
|---|--|
| case m_1 : $s_{V_0^{**},m} = \Gamma^{\parallel} \lambda_{e'} \sqrt{\pi/2} \cdot \operatorname{erfi}(-2e\Phi_0/k_B T) + 1$ | $s_{e',m} = (\Gamma^{\perp} \lambda_{e'} \sqrt{\pi} \cdot \operatorname{erfi}(-e\Phi_0/k_B T) + 1)^{-1}$ |
| case m_2 : $s_{V_0^{**},m} = (\Gamma^{\perp} \lambda_{V_0^{**}} \sqrt{\pi/2} \cdot \operatorname{erfi}(2e\Phi_0/k_B T) + 1)^{-1}$ | $s_{e',m} = \Gamma^{\parallel} \lambda_{V_0^{**}} \sqrt{\pi} \cdot \operatorname{erfi}(e\Phi_0/k_B T) + 1$ |

Fig. 8 illustrates the reasons of this outcome. Here, the $\Phi(x)$ profile calculated without further assumptions using the numerical approach (the dashed black curve) can be applied as a reference to check the accuracy of the analytical profile functions. The comparison shows that an underestimation of the potential profile results from eq. {12}. In contrast, the linear profile (eq. {24}) overestimates the potential at the interface (i.e. at $x = 0$) and underestimates it only for large x values. Here over- and underestimation seem to partly compensate each other with the consequence that the resulting outcomes of the relationships relying on eq. {24} (**Table 4**) appear to be more precise than the ones relying on eq. {12} (**Table 5**).

Nonetheless, eq. {12} does not adequately describe the profile function obtained numerically because of its different slope at the interface which corresponds to the electric field $-E_0$. Indeed, the value obtained with eq. {12} does not match with the corresponding quantity calculated with eq. {4},

^x $\operatorname{erfi}(x) = -i \cdot \operatorname{erf}(i \cdot x)$ (i = imaginary unit) and $\operatorname{erf}(x) = 2/\pi \int_0^x e^{-t^2} dt$

which yields the precise value for E_0 without the use of any assumption or approximation. To overcome this problem, it is convenient to use the following equation

$$\Phi = -\frac{\rho_0}{2\varepsilon_r\varepsilon_0}x^2 - E_0x + \Phi_0, \quad \{25\}$$

for which, at $x=0$, not only $\Phi = \Phi_0$ and $d^2\Phi/dx^2 = -\rho_0/\varepsilon_r\varepsilon_0$ but also $d\Phi/dx = -E_0$ holds (with E_0 being derived from eq. {4}). As illustrated in **Fig. 8**, eq. {25} reproduces the potential profile of the numerical approach much more accurately than eq. {12} and eq. {24}. The integration of eq. {25} inserted in eq. {2} from $x=0$ to the minimum of the parabola at $x_{MS} = \Sigma_{SCL}/\rho_0$ results in eq. {39} and {40} in **Table 6**. Using the numerical approach as a reference, these formulas are found to provide effective conductivity values which are much more accurate compared with those obtained from the equations available in the literature (**Table 4**).

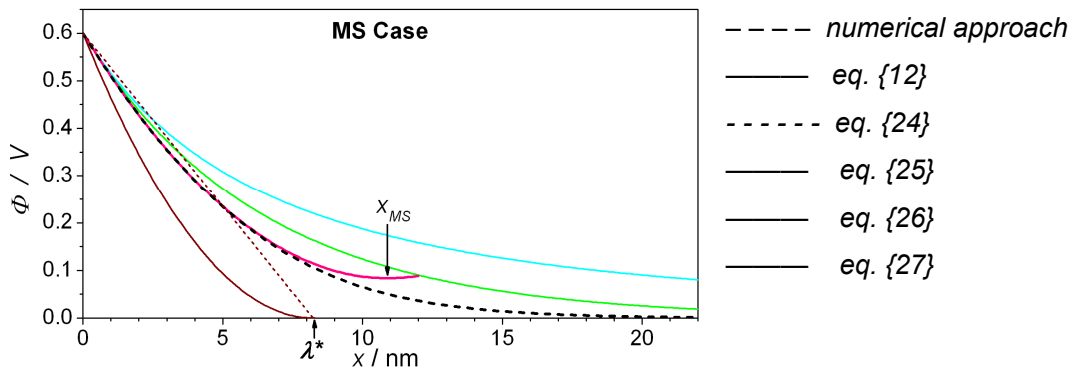


Fig. 8 SCL potential profiles of the MS case: Eq. {12} underestimates the potential profile obtained using the numerical approach whereas eq. {25} deviates less strongly from this curve (and is also more precise than eq. {24}). In addition to eq. {25}, two further profile functions (with $d\Phi/dx = -E_0$ at $x=0$) were tested, which allow for an analytical integration upon insertion in eq. {2}: $\Phi = \Phi_0 \cdot e^{-x \cdot E_0/\Phi_0}$ {26} and $\Phi = 4\Phi_0^3 E_0^{-2} / (x + 2\Phi_0 E_0^{-1})^2$ {27}. However, they describe the potential profile less satisfactorily than eq. {25}. The parameters used in this case are: $\Phi_0 = 0.6$ V, $\varepsilon_r = 26$, $\theta = 700$ °C, $z_{Dop} = -z_{depl} = -1$ and $c_{depl,\infty} = c_{Dop} = 1.25 \cdot 10^{19}$ cm⁻³.

4.3 Mixed Case

Usually, the region in proximity of the border between the GC and MS case, i.e. the mixed case, is treated by simply using the GC solutions.⁴⁴ **Fig. 7** shows, however, that this *modus operandi* generates highly unreliable results. For this reason, a more dependable approach to analytically solve the mixed case is suggested here.

What differentiates the mixed case from the MS case is that in the mixed case the enrichment of the minority charge carrier^{x1} (subscript *enr*) becomes so pronounced close to the interface that its charge density contribution surpasses the one of the immobile dopant: $z_{enr}eC_{enr} > \rho_{IM}$ (see the example profiles given for cases o and p in **Table 4**). Here, the enriched charge carrier dominates the charge density of the space charge zone similarly to the GC case, whilst for larger distances from the interface the charge density is determined by the constant doping content as in the MS case (i.e. $z_{enr}eC_{enr} < \rho_{IM} = \text{const}$).^{x2} Therefore, it is possible to identify a so called transition potential Φ_T , at which $z_{enr}eC_{enr} = \rho_{IM}$.

$$\Phi_T = \frac{k_B T}{-z_{enr} e} \cdot \ln \left[\frac{\rho_{IM}}{z_{enr} e C_{enr, \infty}} \right] \quad \{28\}$$

According to this method, the conductivity effects, i.e. the Σ_i and Ω_i values, can be expressed as the sum of the GC-like contribution (where $|\Phi| > |\Phi_T|$) and the MS-like contribution (where $|\Phi| < |\Phi_T|$).

$$\Sigma_i = \Delta \Sigma_{i,GC} + \Delta \Sigma_{i,MS} \quad \text{and} \quad \Omega_i = \Delta \Omega_{i,GC} + \Delta \Omega_{i,MS} \quad \{29\}$$

For the calculation of the GC-like and the MS-like contributions the same equations and parameters as for the real GC and MS cases can be applied. Further details on the calculation are given in **Table 6**. Despite the complexity of the mixed case, this approach was found to yield very precise results.

^{x1} e.g. the electrons for acceptor doped ceria and positive SCL potentials

^{x2} A further example is given in the mixed case profile shown in Fig. S1 of the Supplementary Information. Here, for $x < 2.5$ nm the enrichment of the minority charge carrier dominates resulting in a steep GC-like charge density profile whilst for $x > 2.5$ nm the charge density profile is rather flat (MS-like).

Table 6 Improved analytical approximations for non-overlapping SCLs. The subscripts i , enr and $depl$ indicate an arbitrary, an arbitrary enriched and an arbitrary depleted charge carrier, respectively, while maj indicates the enriched majority charge carrier in the Gouy-Chapman case.

| Conductivities | |
|---|--|
| <p>The conductivity effects are given in terms of SCL charge contributions Σ_i and reduced resistances Ω_i. In order to determine the normalized conductivities $s_{i,m} = \sigma_{i,m} / \sigma_{i,\infty}$ from these quantities, the geometry of the sample (e.g. microcrystalline pellet or thin film) needs to be taken into consideration. The geometrical factors Γ^{\parallel} and Γ^{\perp} are given in Table 3.</p> | |
| <p>Enriched charge carriers: $s_{i,m} = s_{i,m}^{\parallel}$ with $s_{i,m}^{\parallel} = \Gamma^{\parallel} \cdot \frac{\Sigma_i}{z_i e c_{i,\infty}} + 1$</p> | |
| <p>Depleted charge carriers: $s_{i,m} = s_{i,m}^{\perp}$ with $s_{i,m}^{\perp} = (\Gamma^{\perp} z_i e c_{i,\infty} \Omega_i + 1)^{-1}$</p> | |
| <p>Note that the assumptions $s_{i,m} = s_{i,m}^{\parallel}$ and $s_{i,m} = s_{i,m}^{\perp}$ are valid for $d \gg \ell_{SCL}$. If $d \approx \ell_{SCL}$ (but the SCLs do not yet significantly overlap) then both $s_{i,m}^{\parallel}$ and $s_{i,m}^{\perp}$ contributions become relevant and $s_{i,m} \approx s_{i,m}^{\parallel} \cdot s_{i,m}^{\perp}$ should be applied instead.</p> | |
| Gouy-Chapman Case | |
| <p>In the Gouy-Chapman case, the enriched majority charge carrier should be considered (subscript maj). Its charge contribution is calculated using eq. {31} (or {32}) (for A and λ see the parameters section at the end of this Table). The relationships which need to be applied for the depleted charge carriers and for the enriched minority charge carriers depend on the ratio of their charge number and the charge number of the majority charge carrier (eq. {33}-{38}).</p> <p>The resulting preliminary values Σ'_i and Ω'_i, however, are still rather imprecise and need to be corrected with the factor $\Sigma_{SCL} / \Sigma'_{SCL}$ (eq. {30}). This yields the final quantities Σ_i and Ω_i. Hereby Σ'_{SCL} is simply the sum of all Σ'_i values whereas the SCL charge Σ_{SCL} can be calculated easily using eq. {4}.</p> | |
| Correction | |
| $\Sigma_i = \frac{\Sigma_{SCL}}{\Sigma'_{SCL}} \Sigma'_i \quad \text{and} \quad \Omega_i = \frac{\Sigma_{SCL}}{\Sigma'_{SCL}} \Omega'_i \quad \text{with} \quad \Sigma'_{SCL} = \sum_{i=1}^{N_M} \Sigma'_i \quad \{30\}$ | |
| Enriched Majority Charge Carrier | |
| <p>in general: $\Sigma'_{maj} = z_{maj} e c_{maj,\infty} \cdot 2\lambda (A - 1)$, $\Omega'_{maj} = (z_{maj} e c_{maj,\infty})^{-1} \cdot 2\lambda (A^{-1} - 1)$ {31}</p> | |
| <p>if all Σ'_i except Σ'_{maj} are very small: $\Sigma_{maj} = \Sigma_{SCL}$ {32}</p> | |
| Depleted Charge Carriers | |
| <p>if $\frac{z_{depl}}{z_{maj}} = -\frac{1}{2}$: $\Sigma'_{depl} = z_{depl} e c_{depl,\infty} 2\lambda \ln \left[\frac{1}{2} (A^{-1} + 1) \right]$, $\Omega'_{depl} = (z_{depl} e c_{depl,\infty})^{-1} 2\lambda \ln \left[\frac{1}{2} (A + 1) \right]$ {33}</p> | |
| <p>if $\frac{z_{depl}}{z_{maj}} = -1$: $\Sigma'_{depl} = z_{depl} e c_{depl,\infty} \cdot 2\lambda (A^{-1} - 1)$, $\Omega'_{depl} = (z_{depl} e c_{depl,\infty})^{-1} \cdot 2\lambda (A - 1)$ {34}</p> | |
| <p>if $\frac{z_{depl}}{z_{maj}} = -2$: $\Sigma'_{depl} = z_{depl} e c_{depl,\infty} 2\lambda \left(\frac{A^{-3}}{3} + A^{-1} - \frac{4}{3} \right)$, $\Omega'_{depl} = (z_{depl} e c_{depl,\infty})^{-1} 2\lambda \left(\frac{A^3}{3} + A - \frac{4}{3} \right)$ {35}</p> | |

Further Enriched Minority Charge Carriers

$$\text{if } \frac{z_{enr}}{z_{maj}} = \frac{1}{2} : \quad \Sigma'_{enr} = z_{enr} e c_{enr,\infty} \cdot 2\lambda \cdot \ln \left[\frac{1}{2} (A+1) \right], \quad \Omega'_{enr} = (|z_{enr}| e c_{enr,\infty})^{-1} \cdot 2\lambda \ln \left[\frac{1}{2} (A^{-1}+1) \right] \quad \{36\}$$

$$\text{if } z_{enr} = z_{maj} : \quad \Sigma'_{enr} = z_{enr} e c_{enr,\infty} \cdot 2\lambda (A-1), \quad \Omega'_{enr} = (|z_{enr}| e c_{enr,\infty})^{-1} \cdot 2\lambda (A^{-1}-1) \quad \{37\}$$

$$\text{if } \frac{z_{enr}}{z_{maj}} = 2 : \quad \Sigma'_{enr} = z_{enr} e c_{enr,\infty} \cdot 2\lambda \left(\frac{A^3}{3} + A - \frac{4}{3} \right), \quad \Omega'_{enr} = (|z_{enr}| e c_{enr,\infty})^{-1} \cdot 2\lambda \left(\frac{A^{-3}}{3} + A^{-1} - \frac{4}{3} \right) \quad \{38\}$$

Mott-Schottky Case

Here two different situations can be distinguished. For low SCL potentials (i.e. $e^{|\phi_0/k_B T|} < 4$) the equations of the Gouy-Chapman case have to be applied. For higher SCL potentials the Σ_i and Ω_i values are calculated using eq. {39} and {40}.

Moderate and High Potentials (i.e. $e^{|\phi_0/k_B T|} > 4$)

$$\Sigma_i = z_i e c_{i,\infty} \cdot \left(-x_{MS} - \frac{1}{\rho_0} \cdot \frac{\sqrt{\rho_0}}{\sqrt{z_i}} \cdot \sqrt{\frac{\pi \epsilon_r \epsilon_0 k_B T}{2e}} \cdot e^{\frac{-z_i e}{k_B T} \left(\phi_0 - \frac{x_{MS} E_0}{2} \right)} \cdot \operatorname{erfi} \left[E_0 \frac{\sqrt{z_i}}{\sqrt{\rho_0}} \sqrt{\frac{e \epsilon_r \epsilon_0}{2 k_B T}} \right] \right) \quad \{39\}$$

$$\Omega_i = \frac{1}{|z_i| e c_{i,\infty}} \cdot \left(-x_{MS} + \frac{1}{\rho_0} \cdot \frac{\sqrt{\rho_0}}{\sqrt{z_i}} \cdot \sqrt{\frac{\pi \epsilon_r \epsilon_0 k_B T}{2e}} \cdot e^{\frac{z_i e}{k_B T} \left(\phi_0 - \frac{x_{MS} E_0}{2} \right)} \cdot \operatorname{erfi} \left[E_0 \frac{\sqrt{z_i}}{\sqrt{\rho_0}} \sqrt{\frac{-e \epsilon_r \epsilon_0}{2 k_B T}} \right] \right) \quad \{40\}$$

Note that depending on the sign of ρ_0 and z_i the term $\sqrt{\rho_0}/\sqrt{z_i}$ is not always equal to $\sqrt{\rho_0/z_i}$. For $z_i \cdot \rho_0 < 0$ (e.g. for Σ_i of the depleted charge carrier) the argument of the erfi function becomes imaginary and eq. {39} and {40} can be rearranged according to $\operatorname{erfi}(x) = -i \cdot \operatorname{erf}(i \cdot x)$ (with i being the imaginary unit here).

Low Potentials (i.e. $e^{|\phi_0/k_B T|} < 4$)

This case can be treated using the equations of the Gouy-Chapman case {33}–{38} including the correction {30}. To calculate λ and A with eq. {13} and {43} set $z_{maj} = -\operatorname{sgn}[\phi_0]$ and $z_{maj} e c_{maj,\infty} = \rho_{IM}$.

Mixed Case

In the mixed case firstly the transition potential ϕ_T needs to be determined

$$\phi_T = \frac{k_B T}{-z_{enr} e} \cdot \ln \left[\frac{\rho_{IM}}{z_{enr} e c_{enr,\infty}} \right]. \quad \{28\}$$

For $|\phi| > |\phi_T|$ the profile has the characteristics of the GC case whereas for $|\phi| < |\phi_T|$ it is MS-like. Both contributions sum up to the total Σ_i and Ω_i values.

$$\Sigma_i = \Delta \Sigma_{i,GC} + \Delta \Sigma_{i,MS} \quad \text{and} \quad \Omega_i = \Delta \Omega_{i,GC} + \Delta \Omega_{i,MS} \quad \{29\}$$

The GC-like and MS-like contributions are calculated as follows.

Gouy-Chapman Contributions $\Delta\Sigma_{i,GC}$ and $\Delta\Omega_{i,GC}$

The Gouy-Chapmann like part of the profile is only valid for potentials between ϕ_T and ϕ_0 . Therefore, firstly the values Σ'_{i,ϕ_0} and Ω'_{i,ϕ_0} need to be determined using the equations of the GC case, namely eq. {31} and {33}–{38} (hereby the enriched charge carrier is considered as majority charge carrier; i.e. eq. {31} holds). The Σ'_{i,ϕ_0} and Ω'_{i,ϕ_0} values, however, contain also the part of the profile where $|\phi| < |\phi_T|$ (i.e. the MS-like part). This contribution needs to be subtracted:

$$\Delta\Sigma'_{i,GC} = \Sigma'_{i,\phi_0} - \Sigma'_{i,\phi_T} \quad \text{and} \quad \Delta\Omega'_{i,GC} = \Omega'_{i,\phi_0} - \Omega'_{i,\phi_T} \quad \{41\}$$

For this purpose the values Σ'_{i,ϕ_T} and Ω'_{i,ϕ_T} are calculated using again equations {31} and {33}–{38} in which, nevertheless, ϕ_0 needs to be replaced by ϕ_T . In analogous manner, the value $\Delta\Sigma_{SCL,GC} = \Sigma_{SCL,\phi_0} - \Sigma_{SCL,\phi_T}$ is calculated using eq. {4}. The GC correction is obtained as shown in eq. {42}, yielding the final $\Delta\Sigma_{i,GC}$ and $\Delta\Omega_{i,GC}$ values:

$$\Delta\Sigma_{i,GC} = \frac{\Delta\Sigma_{SCL,GC}}{\Delta\Sigma'_{SCL,GC}} \Delta\Sigma'_{i,GC}, \quad \Delta\Omega_{i,GC} = \frac{\Delta\Omega_{SCL,GC}}{\Delta\Omega'_{SCL,GC}} \Delta\Omega'_{i,GC} \quad \text{and} \quad \Delta\Sigma'_{SCL,GC} = \sum_{i=1}^{N_{Mobile}} \Delta\Sigma'_{i,GC} \cdot \quad \{42\}.$$

Mott-Schottky Contributions $\Delta\Sigma_{i,MS}$ and $\Delta\Omega_{i,MS}$

The MS-like part of the profile is valid for $0 < |\phi| < |\phi_T|$. Hence, the MS contributions $\Delta\Sigma_{i,MS}$ and $\Delta\Omega_{i,MS}$ are determined as described in the above MS section of this table. In this case, ϕ_0 needs to be replaced by ϕ_T in the respective formulas.

Parameters

General case:

$$\Sigma_{SCL} = -\varepsilon_r \varepsilon_0 E_0 \quad \{4\}, \quad E_0 = \text{sgn}[\phi_0] \cdot \sqrt{\frac{2k_B T}{\varepsilon_r \varepsilon_0} \left(\sum_{i=1}^{N_M} (c_{i,0} - c_{i,\infty}) - \frac{\rho_{IM}}{k_B T} \phi_0 \right)} \quad \{21\}$$

$$\rho_0 = \rho_{IM} + e \cdot \sum_{i=1}^{N_M} (z_i c_{i,0}) \quad \{3\}, \quad \rho_{IM} = e \cdot \sum_{j=1}^{N_{IM}} (z_{IM,j} c_{IM,j}) \quad \{5\}, \quad c_{i,0} = c_{i,\infty} \cdot e^{-\frac{z_i e}{k_B T} \phi_0} \quad \{2\}$$

$$\text{Gouy-Chapman case: } \lambda = \sqrt{\frac{\varepsilon_r \varepsilon_0 k_B T}{2 z_{maj}^2 e^2 c_{maj,\infty}}} \quad \{13\}, \quad A = e^{-\frac{1}{2} \frac{z_{maj} e \phi_0}{k_B T}} \quad \{43\}$$

$$\text{Mott-Schottky case: } x_{MS} = \frac{\Sigma_{SCL}}{\rho_0} \quad \{44\}$$

4.4 Accuracy of the Improved Analytical Solutions

The so-obtained new analytical solutions are summarized in **Table 6** while the corresponding conductivity values are displayed in Fig. 9. Notably, thanks to the improved relationships the transition between the GC and MS case is now smooth and without the discontinuities observed previously (compare **Fig. 9** with **Fig. 5**).

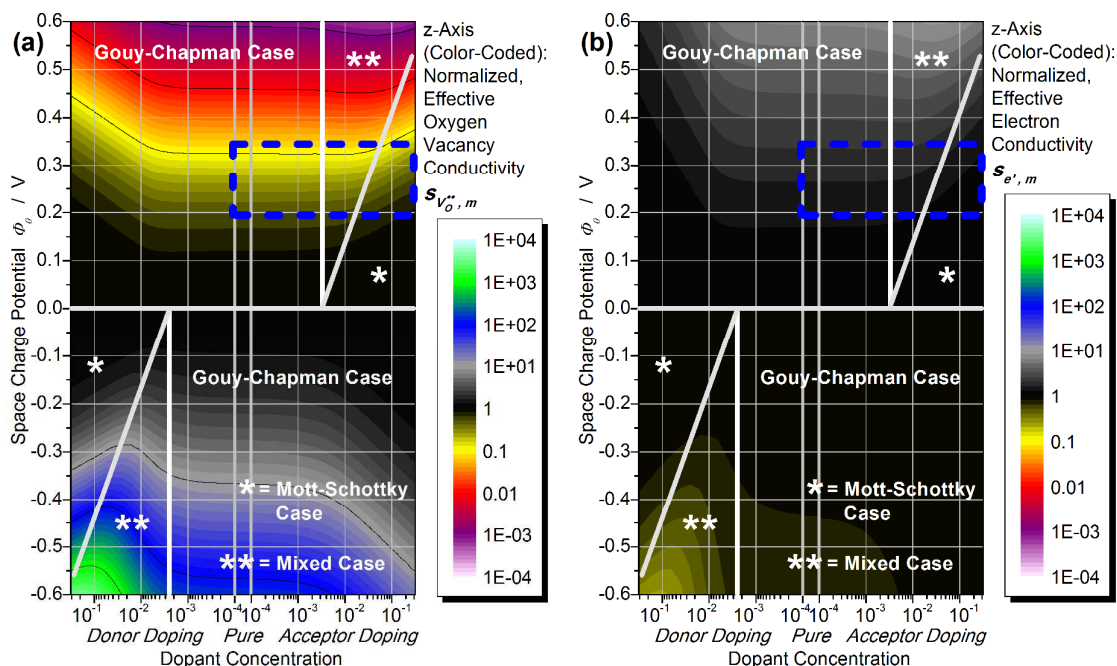


Fig. 9 Normalized effective conductivity of the (a) oxygen vacancies and (b) electrons calculated using the improved analytical solutions given in **Table 6**. The blue rectangle indicates the range of SCL potential (between 0.20 V and 0.34 V) and dopant concentration, which was observed experimentally in nominally pure and acceptor doped ceria.¹⁹⁻²⁴

Fig. 10 displays the deviance between the numerical and the improved analytical approach. Notably, for the improved analytical solutions (for the parameters considered here), the region of low accuracy (3) vanishes, while the region of medium accuracy (2) is considerably reduced compared with **Fig. 7**. Therefore, the deviance is adequately low (uncertainty $< 10\%$) for almost the entire range of space charge potential and dopant concentration considered here. Even for very intricate situations which cannot be treated with the analytical approximation given in the literature (such as low potentials and the mixed case), the improved formulas yield very precise results.

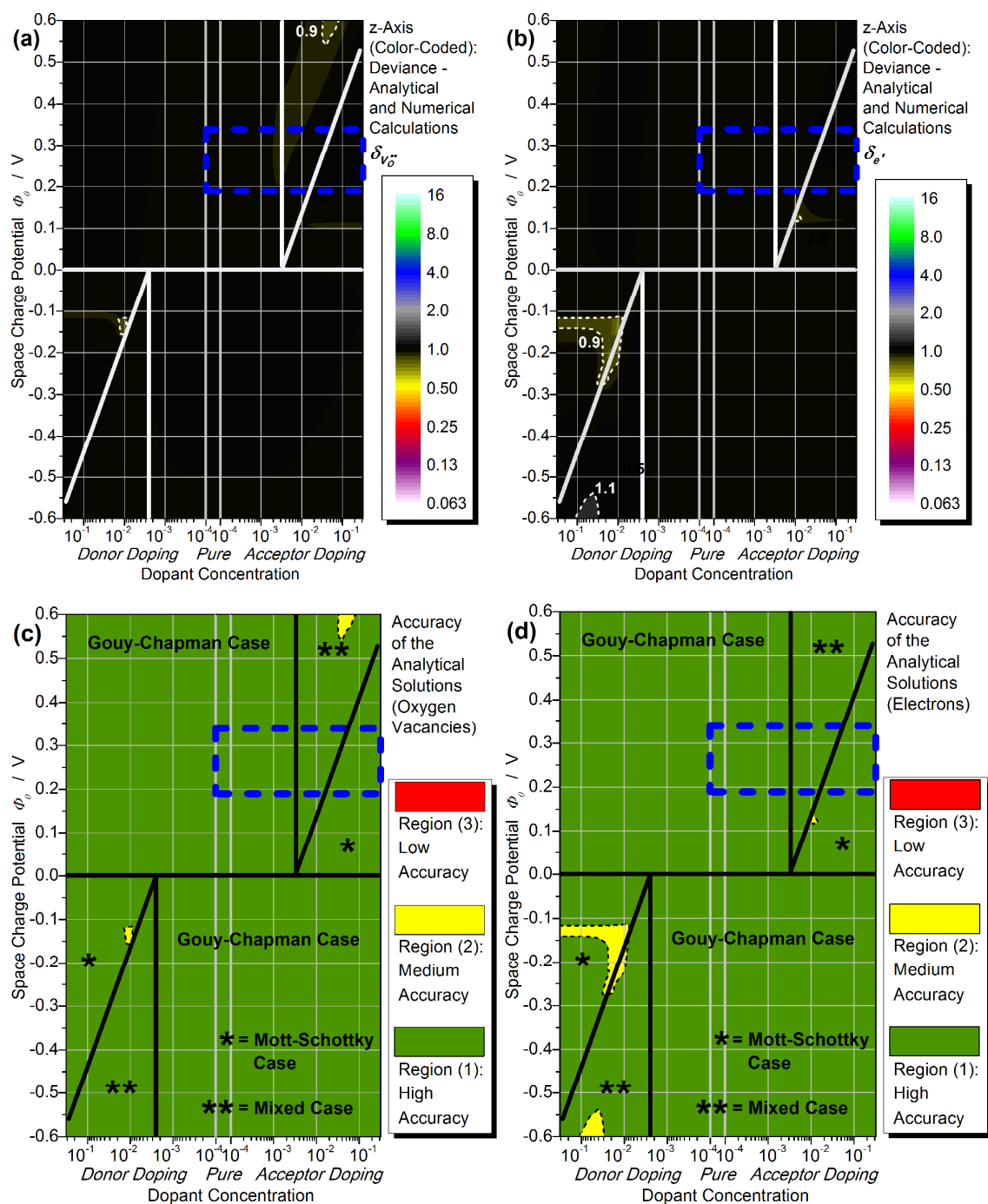


Fig. 10 Panel (a) and (b) illustrate the deviance δ_i between the new analytical (Table 6) and the numerical solutions (as a function of dopant concentration and SCL potential) for oxygen vacancies and electrons, respectively. Panel (c) and (d) show the accuracy map as defined in Fig. 7c and d for the oxygen vacancies and the electrons, respectively.

5 Examples

5.1 Low space charge potentials

In this case, it is worth considering the case of the nanocrystalline ceria films treated in ref. 24 with $d = 16$ nm and $c_{A'} = 10$ %, which at $\theta = 700^\circ\text{C}$ exhibited only a relatively small conductivity change of $s_{V_O^{\bullet\bullet},m} \approx 0.5$. Notably, the values of ϕ_0 obtained numerically and through the improved analytical formulas (**Table 6**) are in very good agreement (0.19 V vs. 0.20 V), whereas the non-improved equations (**Table 4**) yield a rather inaccurate value of 0.25 V.

5.2 Moderate space charge potentials

In a different previous study,²⁰ a rather large SCL potential (0.32 V at $\theta = 700^\circ\text{C}$) was found in ceria films grown on a different substrate (again with $d = 16$ nm and $c_{A'} = 10$ %). For this case, it is worth checking which conductivity values are expected by using the different approaches discussed here.

The numerical solution yields $s_{V_O^{\bullet\bullet},m} = 0.077$, while the improved and the non-improved analytical approximations yield 0.077 and 0.089, which are in excellent and just acceptable agreement with the numerical solution, respectively. For the electrons the situation is comparable and the numerical, improved analytical and non-improved analytical approaches yield the values $s_{e',m} = 2.06$, 2.06 and 1.90, respectively. Hereby, however, the results of the non-improved analytical solutions already include the correction due to the bulk conductivity contribution as explained in the end of Section 1.2 (compare **Fig. 3** with **Fig. 5**). An application of the formulas given in the literature (i.e. a strict use of the equations given in **Table 4**) yields even more unreliable outcomes of $s_{V_O^{\bullet\bullet},m} = 0.098$ and in particular $s_{e',m} = 0.90$.

5.3 Mixed case

Finally, it is worth looking also at samples belonging to the mixed case (between GC and MS situation).²³ To do so, let us consider the same parameters as in the 2 previous examples (namely, $d = 16$ nm, $c_{A'} = 10\%$, $\theta = 700^\circ\text{C}$, $\phi_0 = 0.32$ V) and in a thought experiment decrease the $p\text{O}_2$ until n_∞ increases up to $6 \cdot 10^{19} \text{ cm}^{-3}$. At this point, for $\phi_0 = 0.32$ V, n_0 lies just above the dopant concentration $c_{A'}$. Hence, here the mixed case applies. For such a situation, the improved analytical solution yields $s_{V_O^{\bullet\bullet},m} = 0.076$, which is in good agreement with the numerical solution ($s_{V_O^{\bullet\bullet},m} = 0.083$). In marked contrast, the non-improved solution (including the bulk conductivity correction) is strongly unreliable: $s_{V_O^{\bullet\bullet},m} = 0.025$. A similar outcome is found also for the electrons as

the numerical calculation yields $s_{e,m} = 1.98$, the improved analytical solution $s_{e,m} = 1.96$ and the non-improved $s_{e,m} = 4.38$. Clearly, for the mixed case, the boundary conditions of the non-improved analytical approximations are insufficient, while the improved equations can be dependably employed to determine the effective conductivity values with a good accuracy.

6 Summary

In summary, a numerical approach was used to calculate SCL profiles and determine the expected conductivity changes in CeO_2 . The SCL effects were discussed for the whole dopant range (donor doped, pure and acceptor doped ceria) and as a function of SCL potential ϕ_0 . Using the numerical calculations not only the SCL profiles of the ideal Gouy-Chapman and Mott-Schottky cases could be analyzed but also the more complex mixed cases and SCLs with low potentials.

The accuracy of the analytical approximation equations was tested. Here situations of higher and lower accuracy were found depending on doping level and SCL potential. The approximations were found to be most precise for an enrichment of charge carriers (Gouy-Chapman case), whereas for low potentials and for the transition between the Gouy-Chapman and the Mott-Schottky cases the accuracy was found to be insufficient.

Modifications of the analytical relationships (improved analytical solutions) were proposed which considerably increase the accuracy of the analytical approach. Notably, such improved solutions were found to be precise even for complicated situations, namely the mixed case and low SCL potentials. Finally, three experimental examples were considered, which emphasize the relevance of both the numerical and the modified analytical approach.

Acknowledgements

The authors would like to thank Uwe Traub of the Max Planck Institute for Solid State Research in Stuttgart for the IT support.

References

1. J. Maier, *Ber. Bunsenges. Phys. Chem.* 1986, **90**, 26-33.
2. J. Maier, *Progress in Solid State Chemistry*, 1995, **23**, 171-263.
3. J. Maier, *Physical Chemistry Chemical Physics*, 2009, **11**, 3011-3022.
4. R. A. De Souza, *Physical Chemistry Chemical Physics*, 2009, **11**, 9939-9969.
5. N. Sata, K. Eberman, K. Eberl and J. Maier, *Nature*, 2000, **408**, 946-949.
6. M. C. Göbel, G. Gregori and J. Maier, *Physical Chemistry Chemical Physics*, 2014. (This is Part II of this study)
7. A. Tschöpe, S. Kilassonia and R. Birringer, *Solid State Ionics*, 2004, **173**, 57-61.
8. A. Tschöpe, C. Bäuerle and R. Birringer, *Journal of Applied Physics*, 2004, **95**, 1203-1210.
9. Y. M. Chiang, E. B. Lavik, I. Kosacki, H. L. Tuller and J. Y. Ying, *Applied Physics Letters*, 1996, **69**, 185-187.
10. Y. M. Chiang, E. B. Lavik and D. A. Blom, *Nanostructured Materials*, 1997, **9**, 633-642.
11. Y. M. Chiang, E. B. Lavik, I. Kosacki, H. L. Tuller and J. Y. Ying, *Journal of Electroceramics*, 1997, **1**, 7-14.
12. I. Kosacki, T. Suzuki, V. Petrovsky and H. U. Anderson, *Solid State Ionics*, 2000, **136**, 1225-1233.
13. A. Tschöpe and R. Birringer, *Journal of Electroceramics*, 2001, **7**, 169-177.
14. A. Tschöpe, *Solid State Ionics*, 2001, **139**, 267-280.
15. X. Guo, W. Sigle and J. Maier, *Journal of the American Ceramic Society*, 2003, **86**, 77-87.
16. A. Tschöpe, E. Sommer and R. Birringer, *Solid State Ionics*, 2001, **139**, 255-265.
17. X. Guo and R. Waser, *Progress in Materials Science*, 2006, **51**, 151-210.
18. M. C. Göbel, G. Gregori and J. Maier, *Solid State Ionics*, 2012, **215**, 45-51.
19. S. Kim and J. Maier, *Journal of the Electrochemical Society*, 2002, **149**, J73-J83.
20. M. C. Göbel, G. Gregori, X. Guo and J. Maier, *Physical Chemistry Chemical Physics*, 2010, **12**, 14351-14361.
21. S. J. Litzelman and H. L. Tuller, *Solid State Ionics*, 2009, **180**, 1190-1197.
22. A. Kossoy, Y. Feldman, E. Wachtel, K. Gartsman, I. Lubomirsky, J. Fleig and J. Maier, *Physical Chemistry Chemical Physics*, 2006, **8**, 1111-1115.
23. M. C. Göbel, G. Gregori and J. Maier, *Physical Chemistry Chemical Physics*, 2011, **13**, 10940-10945.

24. M. C. Göbel, G. Gregori and J. Maier, *J. Phys. Chem. C*, 2013, **117**, 22560–22568.
25. H. Inaba and H. Tagawa, *Solid State Ionics*, 1996, **83**, 1-16.
26. B. C. H. Steele, *Solid State Ionics*, 2000, **129**, 95.
27. J. Jacobson, *Chemistry of Materials*, 2009, **22**, 660-674.
28. V. V. Kharton, A. V. Kovalevsky, A. P. Viskup, F. M. Figueiredo, A. A. Yaremchenko, E. N. Naumovich and F. M. B. Marques, *Journal of the Electrochemical Society*, 2000, **147**, 2814-2821.
29. V. V. Kharton, A. V. Kovalevsky, A. P. Viskup, A. L. Shaula, F. M. Figueiredo, E. N. Naumovich and F. M. B. Marques, *Solid State Ionics*, 2003, **160**, 247-258.
30. D. P. Fagg, A. L. Shaula, V. V. Kharton and J. R. Frade, *Journal of Membrane Science*, 2007, **299**, 1-7.
31. X. Zhu and W. Yang, *AIChE Journal*, 2008, **54**, 665-672.
32. A. Leo, S. Liu and J. C. D. da Costa, *International Journal of Greenhouse Gas Control*, 2009, **3**, 357-367.
33. A. Trovarelli, *Catalysis Reviews*, 1996, **38**, 439-520.
34. J. Kaspar, P. Fornasiero and M. Graziani, *Catalysis Today*, 1999, **50**, 285-298.
35. A. Trovarelli, C. de Leitenburg, M. Boaro and G. Dolcetti, *Catalysis Today*, 1999, **50**, 353-367.
36. S. J. Litzelman, R. A. De Souza, B. Butz, H. L. Tuller, M. Martin and D. Gerthsen, *Journal of Electroceramics*, 2009, **22**, 405-415.
37. H. Avila-Paredes and S. Kim, *Solid State Ionics*, 2006, **177**, 3075-3080.
38. P. Lupetin, F. Giannici, G. Gregori, A. Martorana and J. Maier, *Journal of the Electrochemical Society* 2012, **159**, B417-425.
39. G. Gregori, B. Rahmati, W. Sigle, P. A. van Aken and J. Maier, *Solid State Ionics*, 2011, **192**, 65-69.
40. H. L. Tuller and A. S. Nowick, *Journal of the Electrochemical Society*, 1979, **126**, 209-217.
41. M. Mogensen, N. M. Sammes and G. A. Tompsett, *Solid State Ionics*, 2000, **129**, 63-94.
42. H. L. Tuller and A. S. Nowick, *Journal of the Electrochemical Society*, 1975, **122**, 255-259.
43. A. Tschöpe, J. Y. Ying and H. L. Tuller, *Sensors And Actuators B-Chemical*, 1996, **31**, 111-114.
44. S. Kim, J. Fleig and J. Maier, *Physical Chemistry Chemical Physics*, 2003, **5**, 2268-2273.
45. M. C. Göbel, *PhD thesis, University of Stuttgart*, 2013.
46. T. van Dijk and A. J. Burggraaf, *Phys. Stat. Sol. (a)*, 1981, **63**, 229-240.
47. R. Paul, *Halbleiterphysik, Alfred Hüting Verlag, Heidelberg* 1983.